

34

**NASA TECHNICAL
MEMORANDUM**

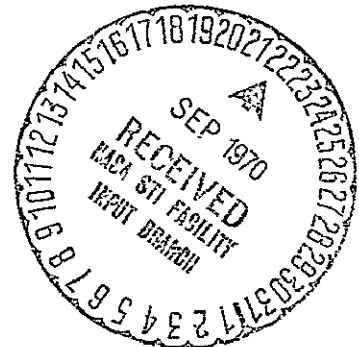
REPORT NO. 53907



**AERODYNAMIC DESIGN AND CALIBRATION OF THE MSFC
THERMAL-ACOUSTIC JET FACILITY - COLD FLOW DUCT**

By K. D. Johnston and W. C. Tidmore
Aero-Astroynamics Laboratory

September 12, 1969



NASA

*George C. Marshall Space Flight Center
Marshall Space Flight Center, Alabama*

MSFC - Form 3190 (September 1968)



FACILITY FORM 602	N70-37529	(THRU)
	51	1
	TMX-53907	11
	(NASA CR OR TMX OR AD NUMBER)	(CATEGORY)

NASA - GEORGE C. MARSHALL SPACE FLIGHT CENTER

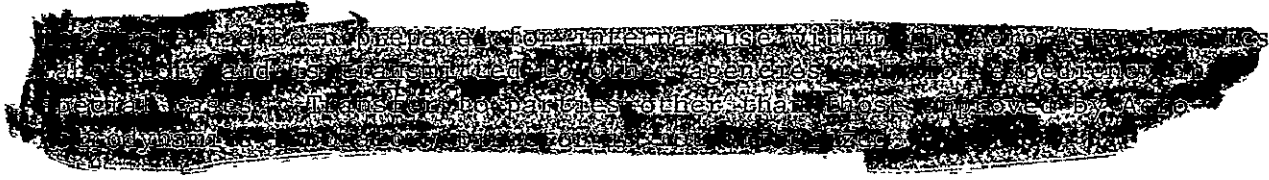
was changed to IN-AERO-69-1
TM X-53907 on September 12, 1969

January 9, 1969

AERODYNAMIC DESIGN AND CALIBRATION OF THE
MSFC THERMAL-ACOUSTIC JET FACILITY - COLD FLOW DUCT

By

K. D. Johnston and W. C. Tidmore*



*Northrop-Nortronics - Huntsville.

FLUID MECHANICS RESEARCH OFFICE
AEROPHYSICS DIVISION
AERO-ASTRODYNAMICS LABORATORY
RESEARCH AND DEVELOPMENT OPERATIONS

ACKNOWLEDGMENT

The authors are grateful to the following persons who contributed to the development of the Cold Flow Duct:

Messrs. R. Felix and E. Simon for allowing Mr. Johnston to provide the design specifications for the Cold Flow Duct to meet the requirements of testing a new optical "crossed-beam" technique for measuring turbulence.

Messrs. H. Belew and J. Clark for coordinating the design and construction of the hardware.

Messrs. E. Simon and J. Heaman for directing the installation, check-out, and operation of the facility.

Mr. J. Sims for designing the nozzle contours and Mr. R. Elkin for computing boundary layer corrections.

The operating crew (Northrop-Nortronics support contractors) for installation and operation of the facility.

LIST OF ILLUSTRATIONS

<u>Figure</u>	<u>Title</u>	<u>Page</u>
1	Thermal-Acoustic Jet Facility Layout (Fig. 9 of NASA TN).....	19
2(a)	The Cold Flow Duct.....	20
2(b)	Test Set-Up Using a Single Nozzle.....	21
3	The Settling Chamber Assenbly.....	22
4	Cross-Section of Settling Chamber.....	23
5	Settling Chamber Rake.....	24
6	Identification of Parts and Instrumentation of the Settling Chamber Assembly (Top View)...	25
7	Nozzles.....	26
8	Typical Schlieren of Neddle Probe in Plume of Cluster Jet.....	27
9	Stagnation Pressure Distributions Across Settling Chamber.....	28
10	Ratio of Wall Static Pressure to Average Rake Pressure in the Settling Chamber.....	29
11	Stagnation Temperature Distributions Across Settling Chamber.....	30
12	Sound Pressure Levels at the Cold Flow Jet Facility (Fig. 12 of NASA TN).....	31
13	Mach Number Characteristics of the Nozzles (Fig. 14 of NASA TN).....	32
14	Effect of Reynolds Number on the Mach Number Distribution in the Nominal Mach 2.46 Nozzle..	33
15	Effect of Reynolds Number on the Mach Number Distribution in the Nominal Mach 3.34 Nozzle..	34

LIST OF ILLUSTRATIONS (Continued)

<u>Figure</u>	<u>Title</u>	<u>Page</u>
16	Shadowgraph of Cluster-Jet Exhaust, $P_0 = 6.205 \times 10^6 \text{ N/m}^2$, Engine 2 and 3.....	35
17	Shadowgraph of Jet Exhaust Mach 2.5, $P_0 = 1.03 \times 10^6 \text{ N/m}^2$ (150 psia).....	36
18	Power Spectrum of Jet Noise at Mike Location 12, $M = 2.46$ Nozzle.....	37
19	Power Spectrum of Jet Noise at Mike Location 1, $M = 3.34$ Nozzle.....	38
20	Power Spectrum of Jet Noise at Mike Location 12, $M = 3.34$ Nozzle.....	39
21	Power Spectrum of Jet Noise at Mike Location 3, $M = 2.46$ Nozzle.....	40
22	Power Spectrum of Jet Noise at Mike Location 4, $M = 2.46$ Nozzle.....	41

DEFINITION OF SYMBOLS

<u>Symbol</u>	<u>Definition</u>
Re	Reynolds number, $\rho UL/\mu$
ρ	density
L	reference length
μ	dynamic viscosity coefficient
M	Mach number
P_c	pressure in settling chamber
D^*	nozzle throat diameter
\dot{m}	mass flow rate
T_c	chamber temperature
ν	kinematic viscosity, μ/ρ
U	mean velocity
ℓ	distance between wire centers of screen (mesh length)
X	distance downstream from screen
X_0	constant distance
A_c	settling chamber cross-sectional area
A^*	nozzle throat area
u	velocity fluctuation
q	dynamic pressure, $\frac{1}{2} \rho U^2$
E	turbulence energy per unit volume
k	pressure drop coefficient of a screen
S(f)	power spectral density
f	frequency

DEFINITION OF SYMBOLS (Continued)

Subscripts

1,2,3 indicate x, y, and z directions, respectively

c denotes settling chamber

Superscripts

* denotes nozzle throat

 denotes time average

AERODYNAMIC DESIGN AND CALIBRATION OF THE
MSFC THERMAL-ACOUSTIC JET FACILITY - COLD FLOW DUCT

SUMMARY

The aerodynamic design of the Cold Flow Duct is reviewed, and some of the data obtained in the calibration test of the facility are presented. The calibration test showed that good control of the settling chamber pressure could be maintained from $0.689 \times 10^6 \text{ N/m}^2$ to $17 \times 10^6 \text{ N/m}^2$, well within the ± 1 percent design limits, and that the facility was generally suitable for a variety of tests requiring a cold jet exhausting into the atmosphere.

I. INTRODUCTION

The Thermal-Acoustic Jet Facility (TAJF) contains hardware for a cold flow jet (designated the "Cold Flow Duct") and a heated flow jet (designated the "Helium Heater"). The two systems provide MSFC with a versatile facility for experimental research on cold or heated jets (up to 1088 °K). In addition to the useful purpose served by each jet alone, the availability of the two control systems makes it possible to study the interaction of hot and cold jets and jets of two different gases. This note describes only the Cold Flow Duct.

The Cold Flow Duct consists of a pressure regulation system, turbulence control assembly, settling chamber, and a contraction section to which a nozzle, or nozzle cluster, can be attached. The working gas can be air at pressures up to about $17 \times 10^6 \text{ N/m}^2$ (depending on mass flow rate) or other gases at pressures up to $10 \times 10^6 \text{ N/m}^2$. The high supply pressures are desired to achieve exhaust jets with high Mach numbers (up to about 4) and large expansion angles so that high altitude plume impingement effects can be partially simulated. The stagnation temperature is always approximately atmospheric or slightly less.

The Cold Flow Duct was designed for jet turbulence and noise studies. However, the system is quite versatile and should be useful for other purposes. The primary features are (1) a large pressure range, (2) variable turbulence, and (3) choice of working gas. Some investigations for which the Cold Flow Duct is suitable are (1) jet noise and turbulence, (2) multiple jet impingement and base flow, and (3) jet impingement on plate or deflector.

II. DESCRIPTION OF FACILITY

A layout of the facility is drawn in figure 1. The Cold Flow Duct is located in the west end of the building, the Helium Heater in the center, and the control and instrumentation room in the east end. The instrumentation room has a double-wall construction and is insulated to reduce the noise level inside.

The test air is supplied by the Test Laboratory's general purpose air storage tanks located about 183 meters (600 feet) west of the TAJF. The average storage pressure of this supply is $22 \times 10^6 \text{ N/m}^2$ (3200 psi). These tanks are connected to the TAJF by two 12.7 cm (5 in) pipes. Four auxiliary storage tanks with a total volume of 136 m^3 (4800 cu. ft.) are located on the north side of the TAJF. However, these tanks are limited to a storage pressure of $12.7 \times 10^6 \text{ N/m}^2$ (1850 psi). The auxiliary tanks can be used to store either air from the Test Laboratory or any other suitable gas which can be brought pre-compressed to the TAJF by truck.

Figure 2 is a photograph of the Cold Flow Duct. The schlieren system (large box frame) which is available for the TAJF is shown pushed forward in its storage position. An optical "crossed-beam" apparatus is shown in the measuring position near the nozzle. An adjustable support which can hold various probes, such as pressure and temperature probes, is also available for this facility. The vacant space in the foreground of figure 2 is now filled by the Helium Heater.

Figure 3 is a close-up photograph of the settling chamber, and figure 4 is a cross-sectional drawing of the settling chamber. The large hole in the settling chamber shown in figure 3 is an access port through which a rake was mounted during the calibration test. A drawing of the rake is given in figure 5. The port could also be used to inject tracers or, conceivably, be used for a low-speed "wind tunnel."

By use of a special extension pipe, the settling chamber can be rolled outside the building to reduce sound reverberation for jet noise tests.

An adapter is available so that all nozzles used on the Cold Flow Duct can also be used on the Helium Heater. Also, the nozzle centerlines of the Cold Flow Duct and Helium Heater are at the same height (123.4 cm above the surface of the supporting rails), and the rails are identical in design so that all instrumentation is interchangeable between the two jets.

III. AERODYNAMIC DESIGN

The aerodynamic design is rather simple. The objective was to provide for exhaust plumes whose Mach numbers, expansion angles, and turbulence levels can be varied over a wide range by using different nozzles, varying chamber pressure, and/or interchanging screens upstream from the nozzle. The design considerations and specifications were given in reference 1.

The following design limits or operating conditions were fixed:

Chamber pressure, $P_c = 0.69 \times 10^6$ to 23.1×10^6 N/m².

Nozzle throat diameter, $D^* = 1.27$ to 5.08 cm (or equivalent for clustered nozzles).

Mass flow rate, $\dot{m} = 2.27$ to 81.66 kilogram/sec.

Chamber temperature, $T_c = 255^\circ\text{K}$ to 322°K .

Because Astronautics Laboratory does not maintain the air supply pressure much over 20.7×10^6 N/m², the maximum operating chamber pressure is approximately 17.2×10^6 N/m².

A. Settling Chamber Design

1. Diffuser

The diffuser (section I of figure 6) is a transition section between the supply pipe and the settling chamber. The airspeed decreases and the static pressure increases in this section causing an unfavorable pressure gradient which tends to separate the flow. However, it was not considered worthwhile to shape the diffuser to prevent separation -- a very small divergence angle would be required [2] -- because the length and cost increases would outweigh the advantages of maintaining attached flow. The mean velocity variations and turbulence introduced by separation can be removed in the settling chamber by screens without undue losses in total pressure. A divergence half-angle of 35 degrees was chosen. A total temperature probe is mounted on a strut in this section.

2. Settling Chamber

The settling chamber (section II of figure 6) consists of a turbulence control assembly and a smooth pipe section downstream. The turbulence control assembly includes a honeycomb and system of screens to produce uniform, low turbulence flow. If higher turbulence levels

are desired, screens can be inserted in a higher velocity region downstream (to be discussed later). The smooth pipe section is necessary to allow the residual turbulence to decay before passing through the nozzle.

The diameter and length of the settling chamber were determined primarily by the requirement of low turbulence at the nozzle entrance. Also, the diameter must be large enough so that the maximum required mass flow can be achieved at sufficiently low speeds so that pressure losses across screens and loads on the screens are not excessive. But the diameter should be small enough to keep wall thickness (determined by structural loads) and fabrication costs within reasonable limits.

a. Length Considerations

Sixty-one centimeters of length in the settling chamber is allowed for the turbulence control assembly. The length of the pipe section is determined by the distance required for the eddies emerging from the last screen in the turbulence control assembly to decay. In the initial period of decay the energy decays inversely with distance downstream the screen [3], i.e.,

$$\frac{\overline{u^2}}{U^2} \propto \frac{1}{\frac{X}{l} - \frac{X_0}{l}},$$

where X_0 is a constant. However, farther downstream, after a transition period, the final period of decay begins in which the decay is much more rapid,

$$\frac{\overline{u^2}}{U^2} \propto \frac{1}{\left(\frac{X}{l} - \frac{X_0}{l}\right)^{5/2}}.$$

The distance required for the final period to set in increases with increasing Re , $U\ell/\nu$, as shown in the following table taken from figures 1, 2, and 3 of reference 4:

$Re, \left(\frac{U\ell}{\nu}\right)$	$\frac{X}{l}$, approximate distance from screen to start of final period of decay.
650	450
950	500
1360	600

Since the largest eddies persist for the longest time, the mesh size of the last screen, which determines eddy sizes, should be small; $\ell = 0.1587$ cm (0.0625 in) was chosen. Using this mesh length, the maximum Re for this settling chamber is on the order of 150,000 which is an order of magnitude greater than that of the above data. Therefore, the final period of decay will begin at much greater distances in the settling chamber. In fact, it is impractical to extend the length to accomplish the desired low turbulence level, because this result can also be accomplished by making the contraction ratio, A_c/A^* , sufficiently large. A length of about 700ℓ is considered appropriate.

$$\text{Length} = 700(0.1587) \approx 111 \text{ cm (44 inches)}.$$

This gives an overall settling chamber length (turbulence control assembly + pipe section) of about 175 cm (69 in). However, about 18 cm (7 in) of this is a contraction section leading to the single nozzle adaptor.

b. Diameter Considerations

Information on how turbulence behaves in a contraction section is limited. Theoretical results in reference 3 indicate that the rms longitudinal component of velocity fluctuations,

$$\sqrt{\mu_1^2},$$

decrease and the rms lateral fluctuations

$$\sqrt{\mu_2^2} \quad \text{and} \quad \sqrt{\mu_3^2},$$

increase across a rapid contraction. This is borne out by experimental evidence in reference 5, except that the lateral fluctuations reach a maximum in the contraction and then decrease rapidly toward the throat. However, in the cold flow jet, the contraction takes place in three stages, and hence does not meet the requirement of being "rapid"; therefore, the behavior of turbulence in the contraction remains in doubt. However, it is believed that opposite changes in

$$\overline{\mu_1^2} \quad \text{and} \quad \overline{\mu_2^2} + \overline{\mu_3^2}$$

will occur, and the resultant rms velocity fluctuation

$$(\overline{\mu_1^2} + \overline{\mu_2^2} + \overline{\mu_3^2})^{1/2}$$

can be assumed roughly constant throughout the contraction. Therefore, the relative turbulence level,

$$(\overline{\mu_1^2} + \overline{\mu_2^2} + \overline{\mu_3^2})^{1/2}/U,$$

decreases markedly as U increases in the contraction section.

A contraction ratio such that the relative turbulence level is decrease by a factor of 1/40 from the settling chamber to the throat of the largest nozzle ($D^* = 5.08$ cm) is considered adequate. Using the continuity equation and the known ratio of densities at nozzle throat to settling chamber, we can obtain the diameter.

$$\frac{U^*}{U_c} = \frac{\rho_c A_c}{\rho^* A^*} = 1.577 \frac{A_c}{A^*} = 40$$

or

$$\left(\frac{D_c}{D^*}\right)^2 = \left(\frac{D_c}{5.08}\right)^2 = 25.37$$

$$D_c = 25.58 \text{ cm (10.07 inches)}.$$

The settling chamber diameter was therefore fixed at 25.4 centimeters (10 inches).

B. Maximum Speed and Dynamic Pressure

Since the settling chamber diameter and maximum mass flow rate have been fixed, the maximum speed and dynamic pressure in the settling chamber can be calculated.

$$U_c = \frac{\rho^*}{\rho_c} \frac{A^*}{A_c} U^* = \frac{\rho^*}{\rho_c} \frac{A^*}{A_c} \sqrt{\gamma R \frac{T^*}{T_c}} \sqrt{T_c}.$$

Thus, V_c depends only on A^* and T_c . Using the maximum values of A^* and T_c ($A_{\max}^* = 20.2 \text{ cm}^2$, $T_{\max} = 322^\circ\text{K}$), we can find the maximum speed in the settling chamber:

$$U_{c_{\max}} = 0.6339 \left(\frac{5.08}{25.4} \right)^2 \sqrt{1.4(R)(.8333)} \sqrt{322} = 8.351 \text{ m/sec} \\ (27.4 \text{ ft/sec}).$$

Now, the dynamic pressure is computed below.

$$q_c = \frac{1}{2} \rho_c U_c^2 = \frac{\gamma}{2} \left(\frac{\rho^*}{\rho_c} \right)^2 \left(\frac{A^*}{A_c} \right)^2 \frac{T^*}{T_c} P_c.$$

Therefore, q_c depends only on A^* and P_c . However, for any given A^* , P_c is limited by the requirement that the mass flow not exceed 81.6 kilograms per second (5.59 slugs per second).

Thus, the maximum operating P_c with $A^* = 20.2 \text{ cm}^2$ is computed below:

$$\dot{m} = \rho^* A^* U^* = \frac{\rho^*}{\rho_c} \frac{\sqrt{\gamma \frac{T^*}{T_c}}}{\sqrt{RT_c}} A^* P_c = 81.56 \text{ kilograms/sec.}$$

or

$$P_{c_{\max}} = \frac{81.56 \sqrt{RT_c}}{A^* \frac{\rho^*}{\rho_c} \sqrt{\gamma \frac{T^*}{T_c}}} = \frac{81.56 \sqrt{R(322)}}{20.2 (.6339) \sqrt{1.4(.8333)}} \\ = 17.8 \times 10^6 \frac{\text{Newton}}{\text{meter}^2} \quad (2580 \text{ psi}).$$

Using $P_{c_{\max}} = 17.8 \times 10^6 \text{ N/m}^2$, we can find the maximum operating dynamic pressure in the settling chamber:

$$q_{c_{\max}} = \frac{1.4}{2} (0.6339)^2 \left(\frac{3.08}{25.4} \right)^4 (0.8333) (17.8 \times 10^6)$$

$$= 6.67 \times 10^3 \frac{\text{Newton}}{\text{meter}^2}.$$

C. Turbulence Control Assembly

The purpose of the turbulence control assembly is to produce uniform flow with only fine scale turbulence which will decay to an acceptable level before passing through the nozzle. The turbulence control devices (see figure 4) consist of a honeycomb at the upstream end of the section and 5 screens of successively finer mesh spaced at 10.16 cm intervals downstream of the honeycomb. The flow approaching the honeycomb has a non-uniform mean velocity profile, V , due to flow separation in the diffuser. Superimposed on the mean flow is intense turbulence which is dominated by large eddies generated in the control valves, pipes, and separated flow.

The effect of the honeycomb is to break up the largest eddies into smaller eddies, damp out transverse fluctuating velocity components, turn the mean flow parallel to the settling chamber walls, and make the mean velocity profile more uniform through frictional resistance. According to reference 1, the average eddy size in a circular pipe may be of the order of 0.15 of the radius. The honeycomb should be several times longer than the mean eddy size; therefore, the length was fixed at 20.16 cm. The honeycomb consists of 0.53 cm diameter holes drilled at approximately 0.71 cm between centers through a 20.16 cm long cylinder. The 0.53 cm hole size was selected so that a typical eddy, whose size is of the order of 2.54 cm, would be forced through several different tubes, thus losing its identity and being broken up into several smaller eddies. However, the wake from the honeycomb cells introduces additional turbulence into the flow, but the eddies thus generated are much smaller than the mean eddy size on the upstream side of the honeycomb. Therefore, a reduction in turbulence at the nozzle is obtained, provided there is a sufficient length of settling chamber, even though the turbulence intensity might be greater immediately downstream of the honeycomb than upstream. This is because small eddies decay faster than large ones [3].

The screens decrease turbulent motions of larger scale than the mesh size and, at the same time, if Re is greater than critical [5], introduce turbulent motions of smaller scale. Although it is desirable to keep Re less than critical (Re_{crit} is of the order of 100 based on mesh length), it is impossible to do so under the specified operating limits of this facility. The mesh size of the most downstream screen was chosen previously as $\ell = 0.1587$ cm. The mesh size and wire diameter are increased successively on each upstream screen as shown in figure 4.

D. Single Nozzle Adaptor

Any desired single nozzle or nozzle cluster configuration can be fitted to the downstream end of the settling chamber. Nozzle clusters can be fitted directly to the end of the settling chamber (Sta. A in figure 6) by means of a "Gray-lock" coupling. The inside diameter at this location is 15.24 cm. The nozzle assembly can be rotated to any desired angular position because there are no bolt holes to match in the Gray-lock coupling method.

To mount a single nozzle, the single nozzle adaptor (section III of figure 6) is used to reduce the inside diameter at the mounting position (Sta. B) to 7.112 cm so that the nozzles will not be unnecessarily large. The single nozzles are also mounted with Gray-lock couplings.

The inside walls at the joints at stations A and B are parallel to the centerline for 3.81 cm on each side of the joint.

An adaptor is available for the Helium Heater, which has a 15.24 cm inside diameter Gray-lock fitting at its downstream end. Therefore, any nozzle which can be fitted to the Cold Flow Duct can also be fitted to the Helium Heater.

E. Turbulence-Generating Screens

If it is desired to create turbulence in the jet core, a coarse screen can be placed at station A or B, or at both places. It seems paradoxical that screens can be used either to damp out turbulence or to generate it. However, by choosing the proper mesh size and location, either of these effects can be attained [7]. We have seen before that the proper method to reduce turbulence is to place fine-mesh screens in a low speed section far upstream of the region where low turbulence is desired. Conversely, to generate turbulence, one can place a coarse screen in a high speed section near the region where a high turbulence

level is desired. In this way, large eddies are created which do not have time to decay before they reach the area of interest. The stream energy per unit volume converted into turbulence is proportional to the dynamic pressure; therefore, it is advantageous to place the screen in a high speed region to create intense turbulence.

$$E = kq. \quad (1)$$

The constant k , usually called the "pressure drop coefficient," is a function only of the screen geometry [2]. Substituting expressions for E and q in the above equation, we get

$$\frac{\sqrt{\mu^2}}{U} = k, \quad (2)$$

where $\sqrt{\mu^2}$ is the resultant rms fluctuating velocity:

$$\sqrt{\mu^2} = \sqrt{\mu_1^2 + \mu_2^2 + \mu_3^2}. \quad (3)$$

The presence of the screen does not decrease the mean dynamic pressure, as can be seen by applying the continuity equation, but the turbulence energy results from a decrease in the static pressure.

From equation 2, to produce a resultant rms velocity fluctuation equal to the mean velocity, a k of one is needed; this need is not at all uncommon. However, because the mean speed increases dramatically in going through a supersonic nozzle, the ratio of

$$\frac{\sqrt{\mu^2}}{U}$$

to U is drastically reduced, assuming

$$\sqrt{\mu^2}$$

remains constant. However, the effect that the passage through a supersonic nozzle has on

$$\sqrt{\mu^2}$$

is unknown.

The screens which are available to insert at stations A and B are listed below:

Station A

meshes per 2.54 cm (1 in)	Wire diameter (cm)	k
10 x 10	0.063	1.3
6 x 6	0.119	2.0
4 x 4	0.160	0.6

Station B

meshes per 2.54 cm (1 in)	Wire diameter (cm)	k
8 x 8	0.063	0.7
6 x 6	0.119	2.0
4 x 4	0.160	0.6

If a turbulence-free jet core is desired, no screen is placed at stations A or B and filler rings are placed in the slots to maintain a smooth wall contour.

F. Nozzles

Any desired single nozzle or nozzle cluster configuration which is consistent with the size and mass flow limitations listed previously may be used on the Cold Flow Duct. However, two existing single nozzles are of special interest because they were designed to produce shock-free jets when run at their design stagnation pressures. These nozzles (shown in figure 7) have exit Mach numbers of 2.46 and 3.34. The schlieren and shadowgraph pictures in reference 8 show that the objective of shock-free plumes was attained. These two nozzles were used in the facility calibration tests.

The nozzle contours, which were computed using the method of characteristics, were corrected for boundary layer displacement thickness following the method of reference 9. The relative size of the two nozzles was chosen so that they produced equal thrust when operated at their design stagnation pressures.

IV. GENERAL DISCUSSION

A. Control System and Mechanical Design

The design of the pressure control system and the hardware were performed by the Hayes International Corporation under contract to the Manufacturing Engineering Laboratory. The pressure regulation system is analyzed in reference 10. Because of the large mass flow range which was required, two control circuits were used (see figure 1). The low flow rate circuit is used for mass flows in the range $0 \text{ kg/sec} \leq \dot{m} \leq 4 \text{ kg/sec}$, and the high flow rate circuit for $4 \text{ kg/sec} \leq \dot{m} \leq 82 \text{ kg/sec}$.

B. Contamination of Jets

The primary use envisioned for the Cold Flow Duct, at least initially, was for research involving optical techniques. For some applications, it is desirable to have the jet free of solid and liquid particles. Therefore, precautions were taken to minimize the particles in the flow. All hardware downstream of the shut-off valves (valves 3 and 4 in figure 1) is made of stainless steel to prevent corrosion and the consequent roughening of the walls and contamination of the flow with rust particles. Also, the compressed air supplied by the Test Laboratory is dried to a specific humidity of approximately 10^{-6} to 3×10^{-6} , so that practically no corrosion occurs in the supply pipes. Keeping the supply air at this low moisture content also limits the formation of water droplets in the jet core to negligible proportions. However, because moist air is entrained in the turbulent shear layer of the jet and because the jet is necessarily cold, condensation of water droplets in the shear layer is unavoidable. If an experiment requires the jet to be free of water drops, then the heater should be used. If the chamber pressure, P_c , exceeds about 6.2×10^6 to $8.2 \times 10^6 \text{ N/m}^2$ (depending on T_c), the equilibrium liquefaction temperature of air is reached in the jet core (see a temperature-entropy diagram for air). The liquid air phenomenon is easily visible at pressures of $8.2 \times 10^6 \text{ N/m}^2$ and above.

It is sometimes desirable to introduce a contaminant in the jet to act as a tracer. A system is available for injecting a volatile liquid, with solid particles suspended in it, into the auxiliary air storage tanks. The liquid droplets evaporate leaving the solid particles suspended in air. This system has been used to inject teflon particles suspended in freon for an optical "crossed-beam" test in which light scattering from the particles produced the desired attenuation of light beams. A tracer injector is also being developed to inject particles in solid form into the flow just upstream of the settling chamber.

If particles are desired only in the jet shear layer, the condensation droplets might be sufficient. However, it is unlikely to obtain a uniform concentration of tracer particles across the shear layer either from water vapor condensation or tracer injection, because the turbulent mixing in the shear layer of "traced" air with "un-traced" air produces a gradient in tracer concentration.

C. Instrumentation

The only permanent items of instrumentation on the Cold Flow Duct are the total temperature probe (item #1 in figure 6) and the wall pressure measurement in the settling chamber (item #2). However, other instrumentation was used during the calibration testing, and it can be used, if desired, for any experiment. The instrumentation is listed and discussed below:

1. Total Temperature Probe (Item #1) - Type: Conax Copper-Constantan Thermocouple - Accuracy of Measurement $\approx \pm 0.55^\circ\text{K}$ from 215°K to 360°K

This thermocouple is mounted on a pipe at the entrance to the diffuser. The thermocouple is in a region of near-stagnant air because of the presence of the pipe. In any case, the static temperature in this section does not vary significantly from total temperature because the flow is in the low subsonic range. The temperature probe was not installed downstream of the screens because it was desired to avoid creating flow disturbances there.

2. Wall Pressure Measurement (Item #2)

A pressure transducer is attached to the outside wall of the settling chamber for measuring the settling chamber static pressure. This measurement is used both to control and record the settling chamber pressure. By interchanging pressure transducers for different ranges of pressure, the chamber pressure can be controlled so that the maximum deviations from the mean are less than ± 0.3 percent of the mean pressure.

3. Fluctuating Pressure Transducer (Item #3) - Type: Kistler Model 601 L (0.063 cm dia.)

This transducer was used to measure the wall pressure fluctuations in the settling chamber during the calibration test.

4. Pressure and Temperature Rake (Item #4)

This rake consists of 6 temperature probes and 5 pitot pressure probes. It was used during the calibration test to verify that (1) the flow is uniform across the settling chamber, (2) the wall static pressure could be assumed equal to the stagnation pressure with acceptable accuracy for pressure control purposes, and (3) the stagnation temperature measured upstream the honeycomb and screens is approximately equal to that obtained in the settling chamber; i.e., the heat transfer to or from the honeycomb and screens is negligible. For normal testing, this rake is removed, leaving the settling chamber unobstructed and the walls smooth.

5. Static Pressure Tubes (Item #5)

Static pressure tubes were used to measure the static pressure distribution along the walls of the Mach 2.46 and 3.34 nozzles.

6. Fluctuating Pressure Transducer (Item #6) - Type: Kistler Model 601 L

Purpose: To measure the wall pressure fluctuations near the exit plane of the nozzle.

7. Pressure Tubes (Item #7)

Pressure tubes are placed just upstream and downstream of stations A and B to obtain wall pressure measurements when screens are used at these locations. Using these measurements, the stagnation pressure downstream of the screens can be estimated by subtracting the pressure drops across the screens from the measured settling chamber pressure.

8. Microphone - Type: Bruel and Kjaer Model 4135

The microphone was placed at different locations about the jet during the calibration test to monitor the sound intensity.

9. Schlieren System - Type: Unertl

The schlieren system is mounted on a large box frame which can be rolled to the desired location at the jet or back into its storage position (see fig. 2). It has a circular field of view (dia. = 15.2 cm, nominally).

D. Facility Operation

A preliminary operation manual for the Cold Flow Duct was prepared by Hayes International [11], and it is expected that the manual will be revised and expanded for this facility by R-AERO-AE personnel.

The operation and performance of the facility have proved quite satisfactory. The compressed air supply is adequate. Sufficient air has normally been available to run as long and frequently as desired. Figure 8 shows a typical schlieren made in the TAJF.

V. CALIBRATION TEST

Shakedown runs on the Cold Flow Duct were begun in September 1966. The operation of the pressure control system was first checked out, and then the tests described below were performed. An extensive quantity of data was obtained of which only a small, representative amount is presented in this note.

Unfortunately, the filler rings at stations A and B were inadvertently omitted during this test, leaving large circumferential slots. It is believed that the presence of these slots did not significantly affect the data. A limited amount of data was later obtained with the slots filled for comparison with the earlier data.

A. Measurements in Settling Chamber

1. Rake Data

Figure 9 shows typical stagnation pressure distributions across the settling chamber which were obtained by the rake for different stagnation pressures. These measurements were made using both the Mach 2.46 and 3.34 nozzles and with all screens installed in the turbulence control assembly. The results show that there were no appreciable variations in pressure across the settling chamber, which, of course, was to be expected.

Figure 10 gives the ratio of the wall static pressure to the average rake pressure (average over all probes) as a function of the rake pressure. Data for both nozzles are included. The bulk of these data is in the range 0.995 to 1.005. The variations in $P_{wall}/P_{rake\ avg.}$ are considered to be within the measuring accuracy of the pressure

transducer system which was used. Therefore, the stagnation pressure can be considered equal to the measured wall static pressure without any correction. This result was expected since the maximum speed in the settling chamber is quite low.

Figure 11 shows typical stagnation temperature distributions across the settling chamber. The maximum deviations of about ± 0.55 °K are considered to be within the measurement accuracy of the thermocouples. The stagnation temperature measured upstream of the turbulence control assembly was usually within ± 3.3 °K of the rake measurements. There was no consistent trend in the difference between T_1 (temperature in diffuser) and T_{rake} . For some runs, T_1 could be as much as 3.3°K greater than T_{rake} . The magnitude of T_1 usually varied less than ± 0.28 °K about the mean during a run.

2. Fluctuating Pressures

The fluctuating pressures measured at the wall of the settling chamber, P_1 , are presented in figure 12 in decibels as a function of the stagnation pressure. The db levels were considerably higher for the Mach 2.46 nozzle than for the Mach 3.34 nozzle. However, the Mach 2.46 nozzle has a larger throat area and therefore has a greater mass flow. It is interesting that the db level reaches a peak, at least for the Mach 2.46 nozzle, at about 5.5×10^6 N/m² and decreases with increasing pressure (and mass flow rate) thereafter.

The spectral analysis of the above wall pressure fluctuations was presented in reference 12. Most of these data had a peak at about 5000 cps. Reference 12 also gives the spectral analysis of the output of an accelerometer which was attached to the outside wall of the settling chamber.

B. Measurements of Nozzle Flow Field

It is believed that the two nozzles used in this test will be of interest to other experimenters because it is possible to achieve shock-free jets with them. Therefore, some of the experimental data on these nozzles are presented.

Figure 13a shows the Mach number profiles along the walls of the two nozzles as determined by static pressure measurements. These data are given with and without the circumferential slots at stations A and B. The presence of the slots had no appreciable effect on the Mach number profiles. The cause of the upturn in indicated Mach number near the exit of the Mach 3.4 (design Mach number) nozzle is not known. However,

since it was consistent throughout the calibration test at various stagnation pressures, it might be a real effect. Figure 13b shows the Mach number distributions, determined from the pitot pressure rake measurements of reference 13, across the nozzle exit planes. Both sets of data show that the actual Mach numbers obtained at the nozzle exits were slightly less than the design values, i.e., $M = 2.5$ and 3.4 . The approximate Mach numbers obtained by averaging these results are 2.46 and 3.34 . The discrepancies were perhaps partially caused by inadequate correction for boundary layer displacement thicknesses since errors of 0.066 cm ($M = 2.5$ nozzle) and 0.0736 cm ($M = 3.4$ nozzle) at the nozzle exits would account for the observed effects.

Figure 14 shows that the Mach number along the wall of the nominal Mach 2.46 nozzle increases with increasing Reynolds number. This is consistent with a thinner boundary layer at higher Reynolds number. The downturn in Mach number near the nozzle exit at $P_c = 6.89 \times 10^5$ N/m² indicates boundary layer separation. Figure 15 gives similar data for the nominal Mach 3.34 nozzle. The variation in Mach number is not nearly so large as for the Mach 2.46 nozzle; however, neither is the Reynolds number variation.

Detailed pitot pressure and stagnation temperature profiles in the jets from the two nozzles are given in reference 13 for several stagnation pressures, P_c .

C. Noise Produced by the Jets

The noise levels measured at two locations near the jets are given, for both nozzles, as a function of chamber pressure in figure 12. The noise levels at several other positions are given in reference 14. The microphone was mounted at the same elevation as the nozzle. For a given location and chamber pressure, the Mach 2.46 nozzle produced more noise than the Mach 3.34 nozzle. The minima at position no. 1 at the chamber pressures corresponding to the design (no-shock) valves are interesting. The noise at this location appears to be dominated by the interaction of the lip shock with the turbulent shear layer, which can be readily seen in shadowgraphs that show sound waves emanating from the shock-shear layer intersection position. When the shock wave is removed by changing P_c to the design value, the sound level is reduced. Figure 16 shows the sound waves emitted by the cluster jet model as seen by the shadowgraph technique. Figure 17 is a shadowgraph showing the jet exhaust from a single nozzle

The power spectrum of the noise measured at mike location 12 (see figure 12 for mike position) is given in figure 18 for the Mach 2.46 nozzle operating at $P_c = 1.58 \times 10^6 \text{ N/m}^2$, the design stagnation pressure. These data were obtained using an Allison one-third octave frequency analyzer. The use of this machine is described in reference 12. The power spectrum is rather peaked with the peak occurring at about 1000 cps. The mean square sound pressure level can be found by taking the area under the $S(f)$ curve;

$$\overline{p^2} = \int_0^{\infty} S(f) df.$$

This integration was performed mechanically using a planimeter. The results were converted to decibel form;

$$\text{db} = 20 \log_{10} \frac{\sqrt{\overline{p^2}}}{p_{\text{ref}}},$$

where

$$p_{\text{ref}} = 0.00002 \frac{\text{Newton}}{\text{meter}^2}.$$

The sound pressure level at this location obtained by the above method was 147 db. This compares with 149 db obtained with an rms meter. This is a satisfactory agreement considering the possible errors involved in the two methods.

The power spectrum of the noise at mike location 1 is given in figure 19 for the Mach 3.34 nozzle at $6.55 \times 10^6 \text{ N/m}^2$. The peak in the power spectrum occurred at the same frequency as in figure 18, although the Mach number, chamber pressure, etc., were different. Similar data are given in figure 20 at mike location 12 for the Mach 3.34 nozzle. Comparison of figures 19 and 20 reveals the strong dependence of sound pressure level on position along the jet, the level being much higher 1.524 m downstream from the nozzle than near the nozzle exit.

Figures 21 and 22 give the power spectra of the noise measured 3.35 and 4.87 m, respectively, from the Mach 2.5 jet centerline at 15.24 cm downstream of the nozzle exit. The sound pressure level falls off markedly at this distance from the jet.

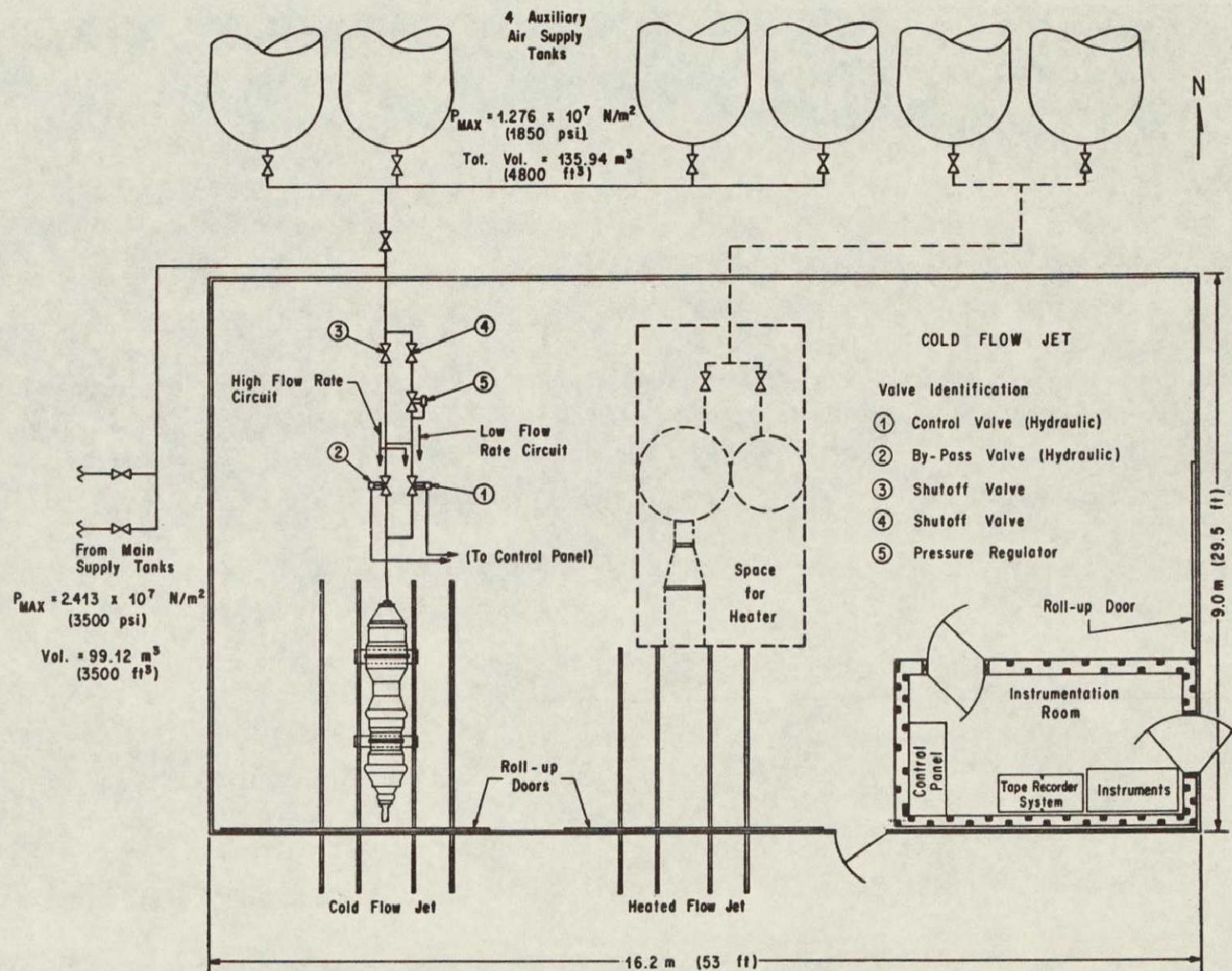


FIG. 1. THERMAL ACOUSTIC JET FACILITY LAYOUT

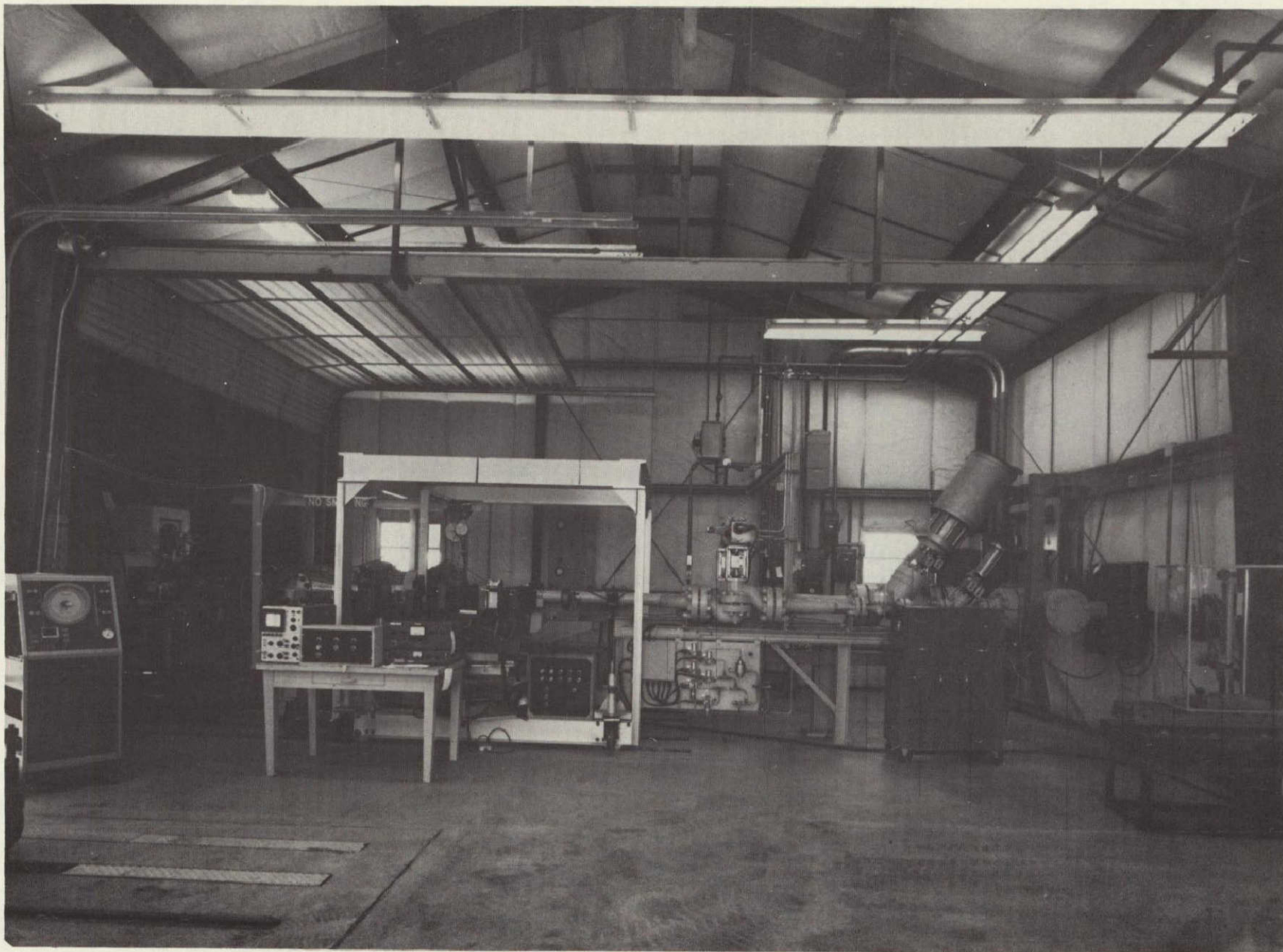


FIG. 2(a). THE COLD FLOW DUCT

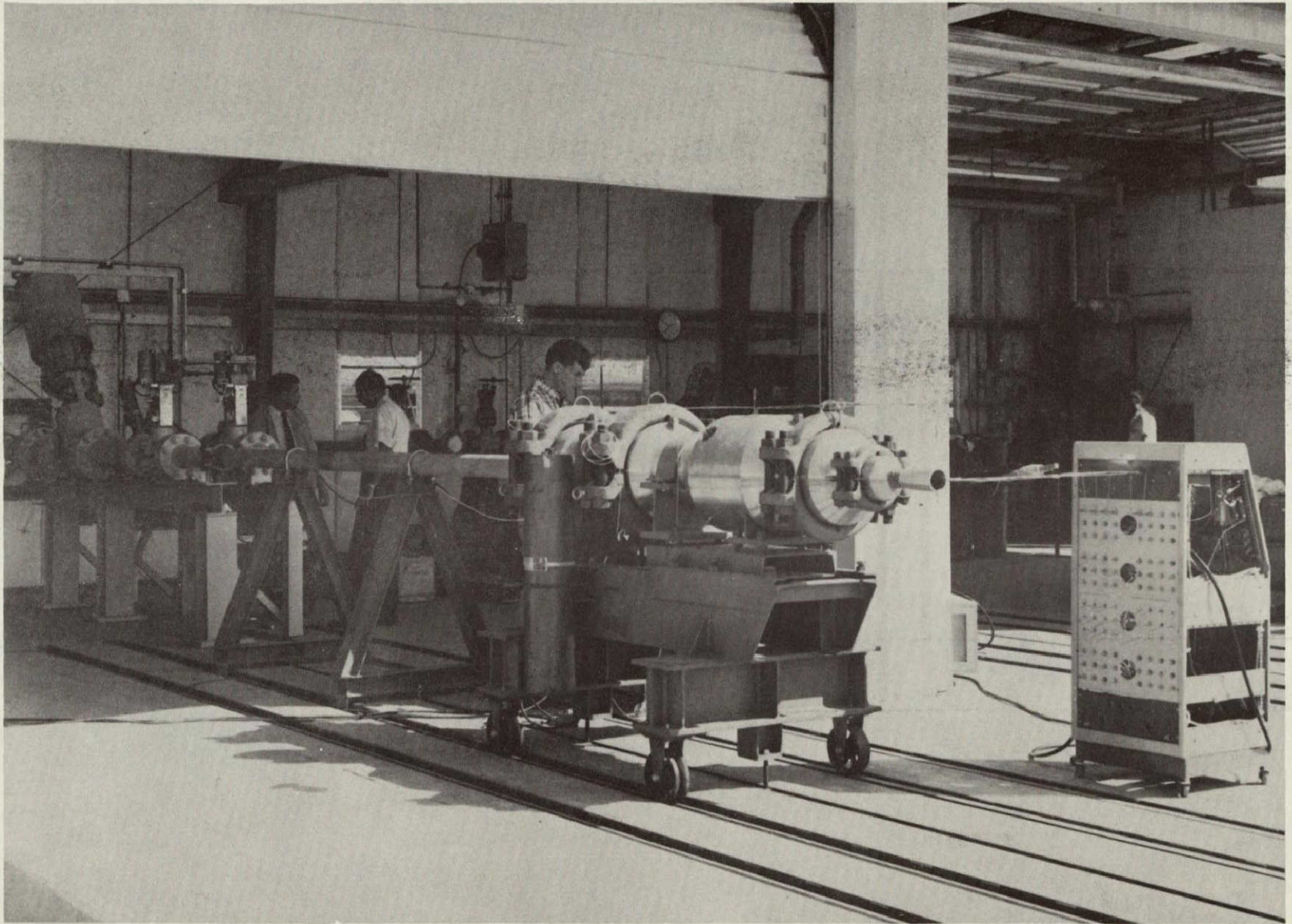


FIG. 2 (b). TEST SET-UP USING A SINGLE NOZZLE

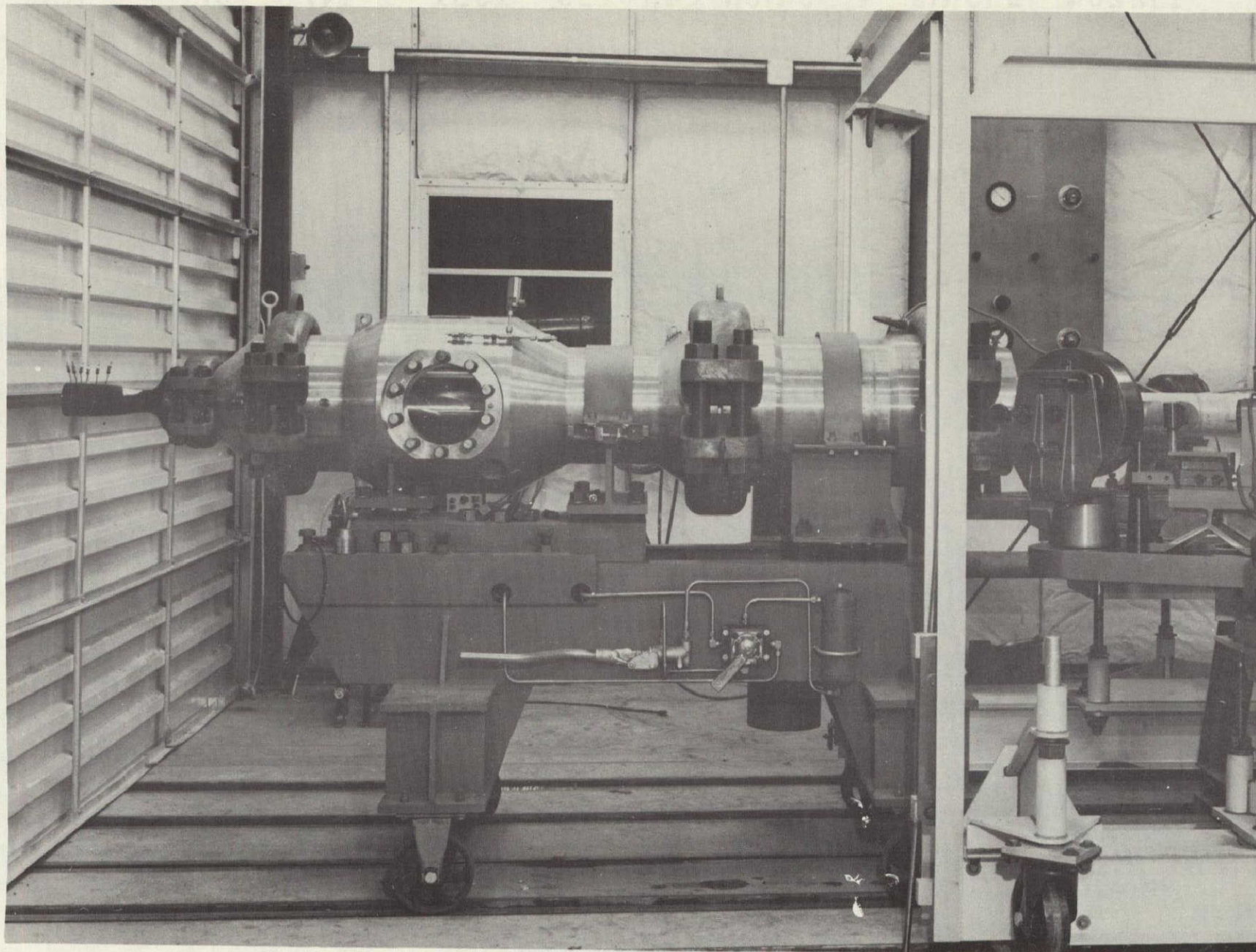


FIG. 3. THE SETTLING CHAMBER ASSEMBLY

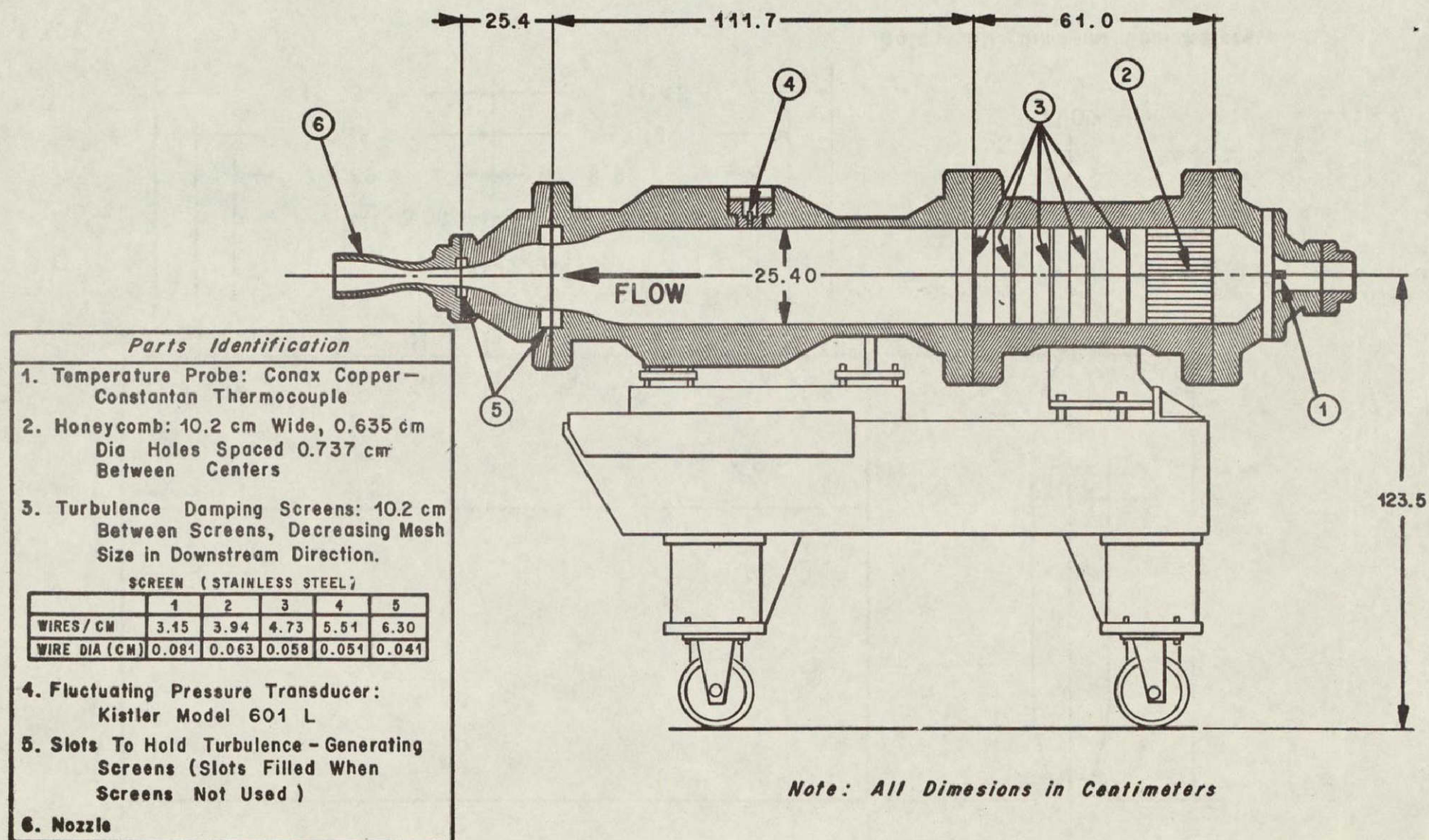


FIG. 4. CROSS-SECTION OF SETTLING CHAMBER

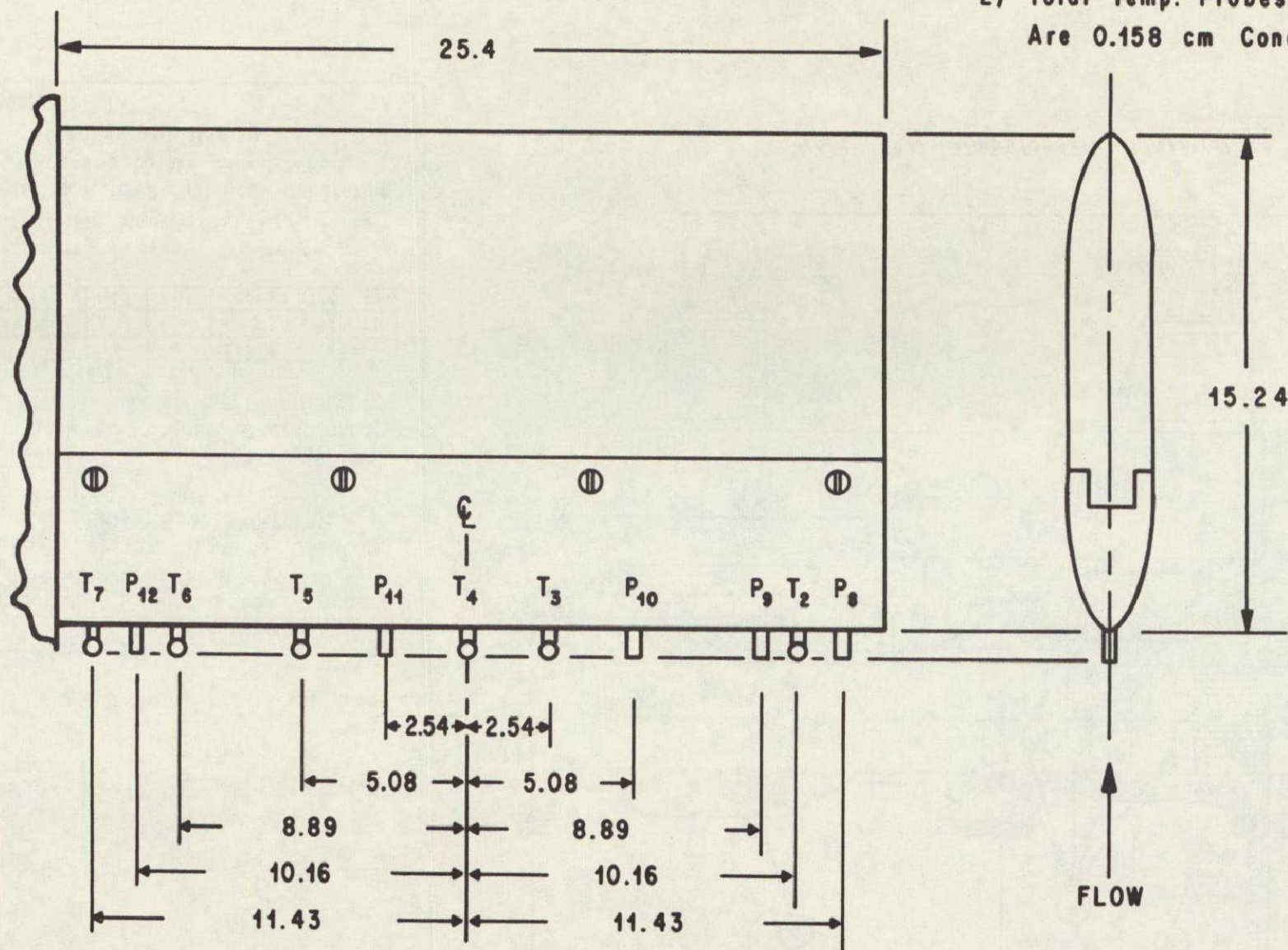
Note :

1) Total Pressure Probes

Are 0.158 cm OD \times 0.0865 cm ID

2) Total Temp. Probes

Are 0.158 cm Conax Thermocouples

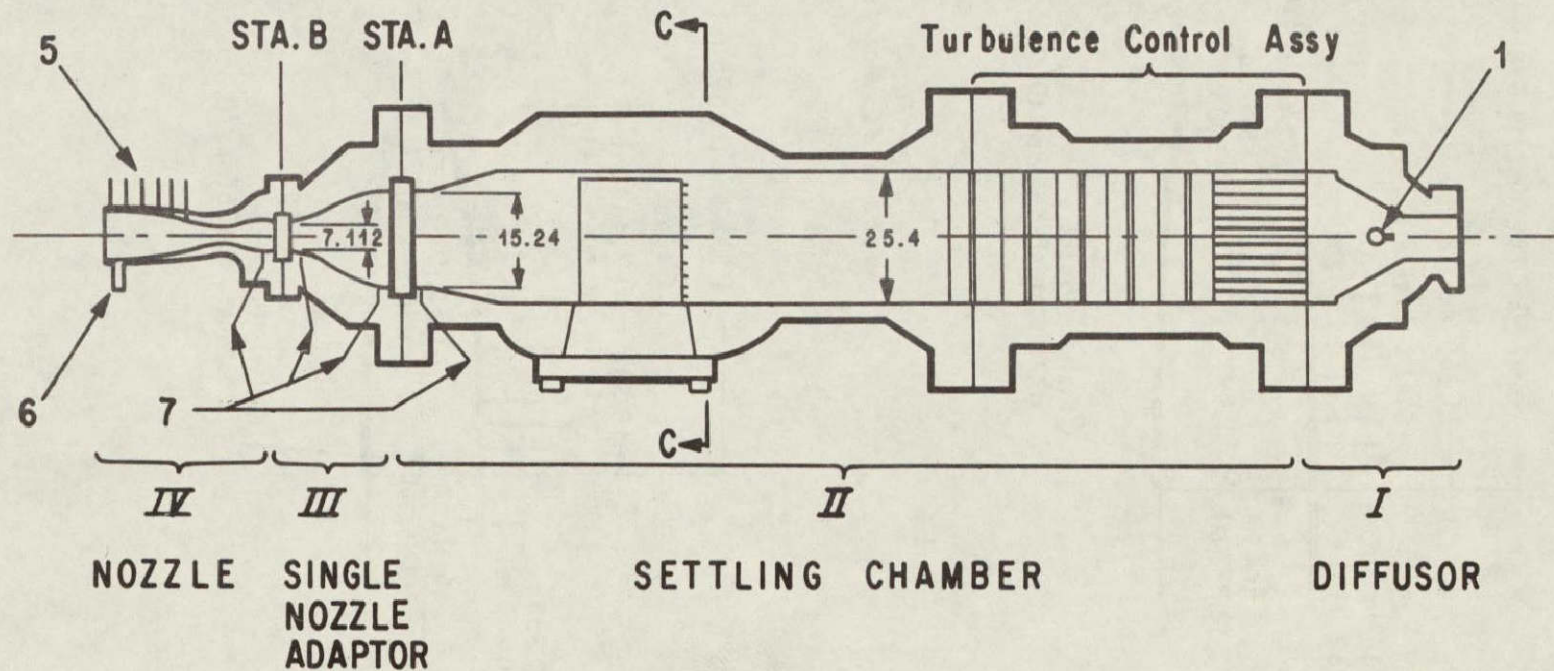
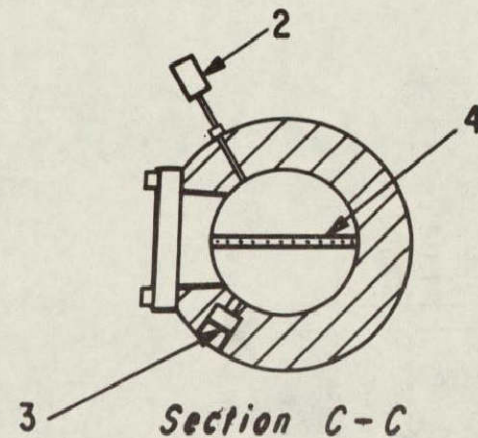


Note: All Dim. in Centimeters

FIG. 5. SETTLING CHAMBER RAKE

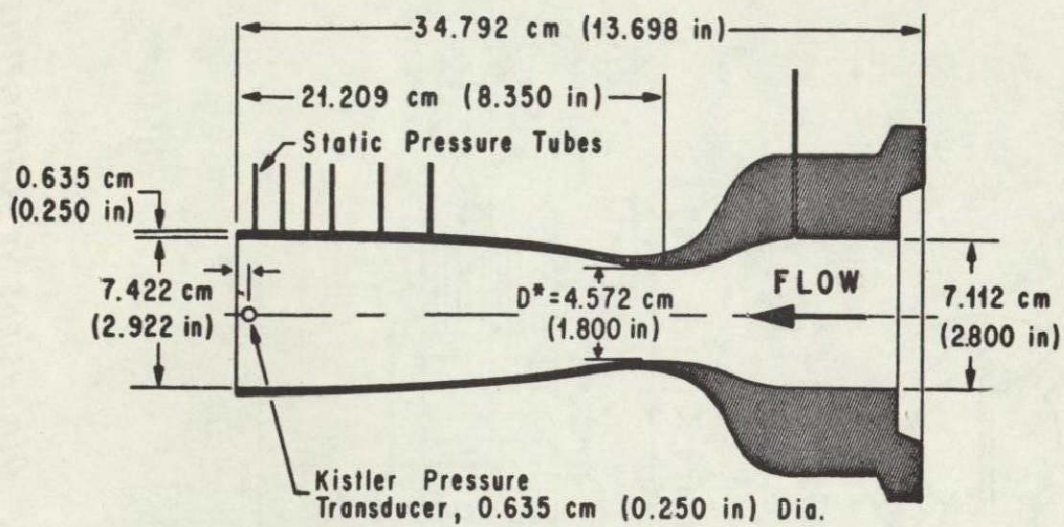
LEGEND:

1. Total Temperature Probe
2. Settling Chamber Static Pressure (Also Control Pressure Transducer)
3. Fluctuating (or Dynamic) Pressure Transducer
4. Settling Chamber Rake (See Fig. 5)
5. Static Pressure Tubes
6. Dynamic Pressure Transducer
7. Static Pressure Tubes

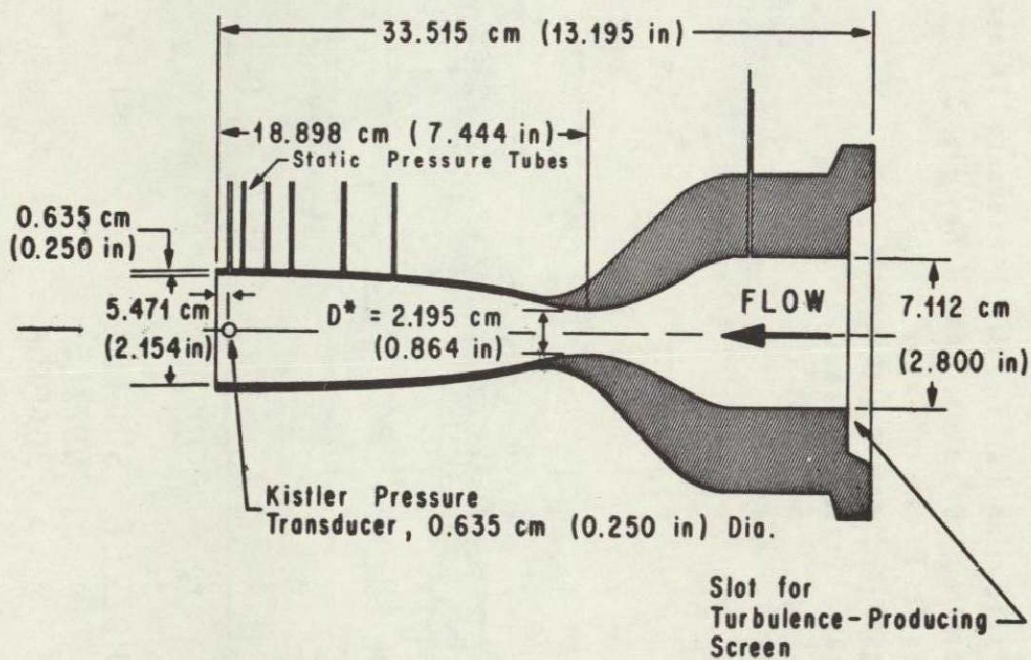


NOTE: All Dimensions in Centimeters

FIG. 6. IDENTIFICATION OF PARTS AND INSTRUMENTATION OF THE SETTLING CHAMBER ASSEMBLY (TOP VIEW)



Mach 2.46 Nozzle



Mach 3.34 Nozzle

FIG. 7. NOZZLES

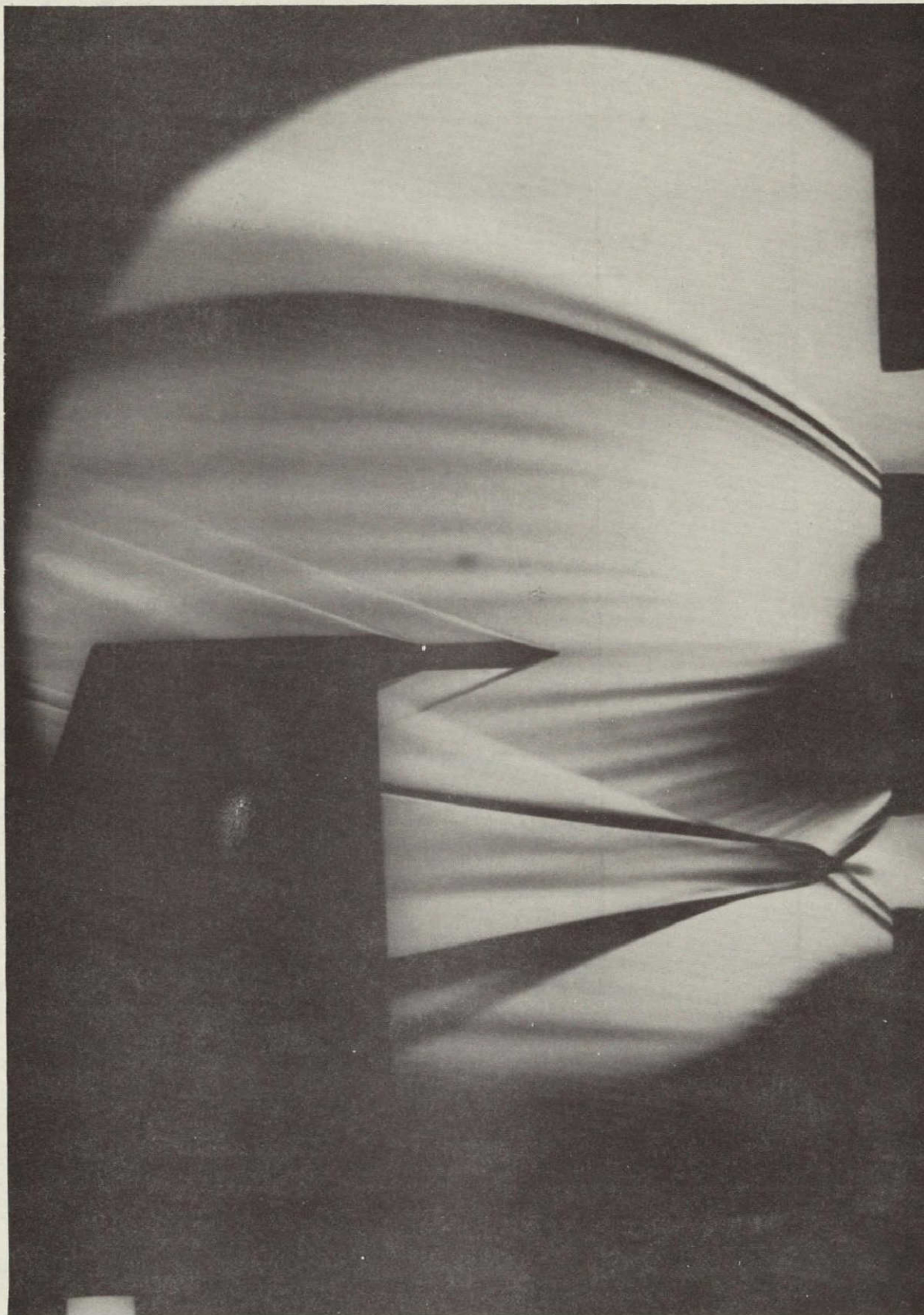


FIG. 8. TYPICAL SCHLIEREN OF NEEDLE PROBE IN
PLUME OF CLUSTER JET

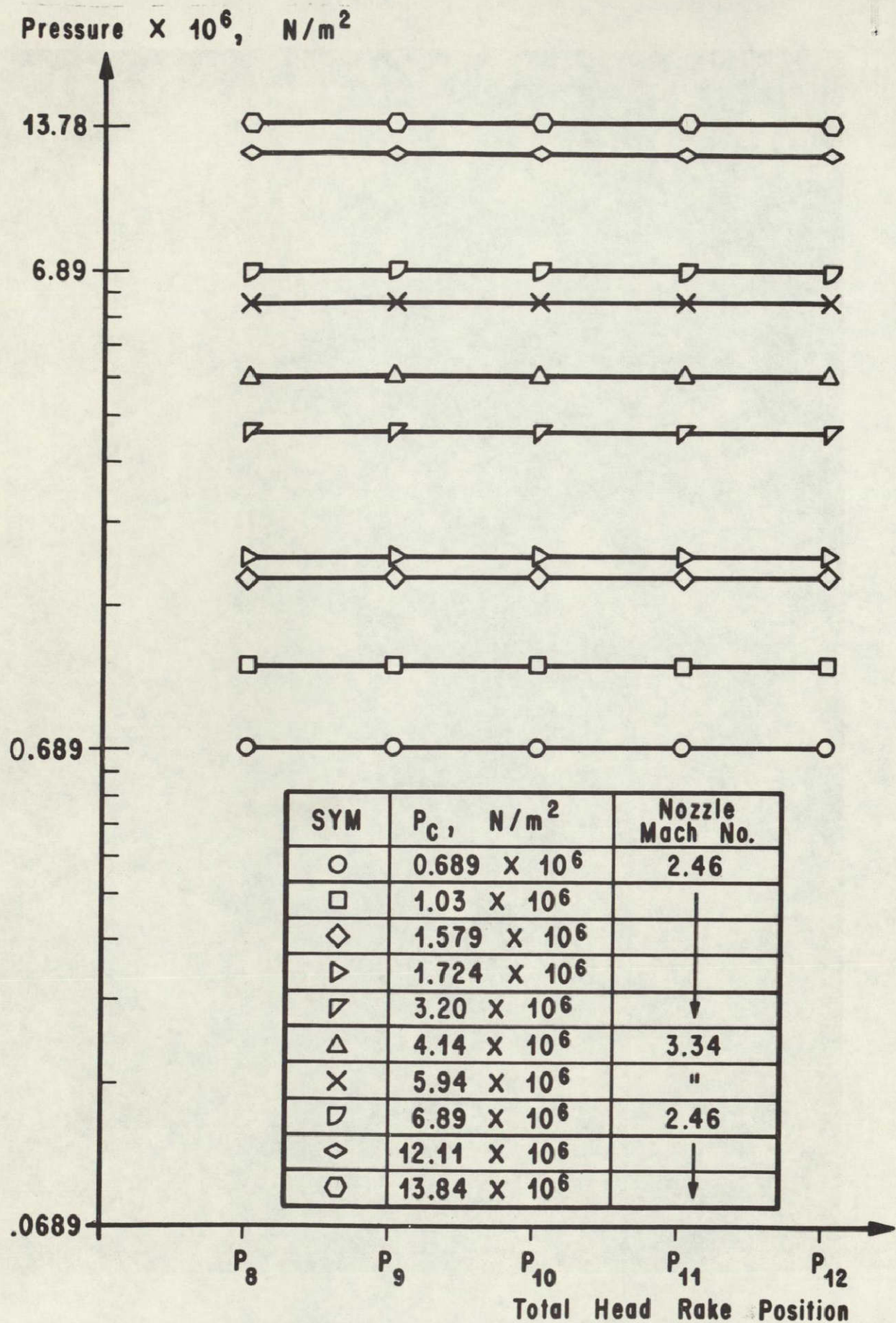


FIG. 9. STAGNATION PRESSURE DISTRIBUTION ACROSS SETTLING CHAMBER

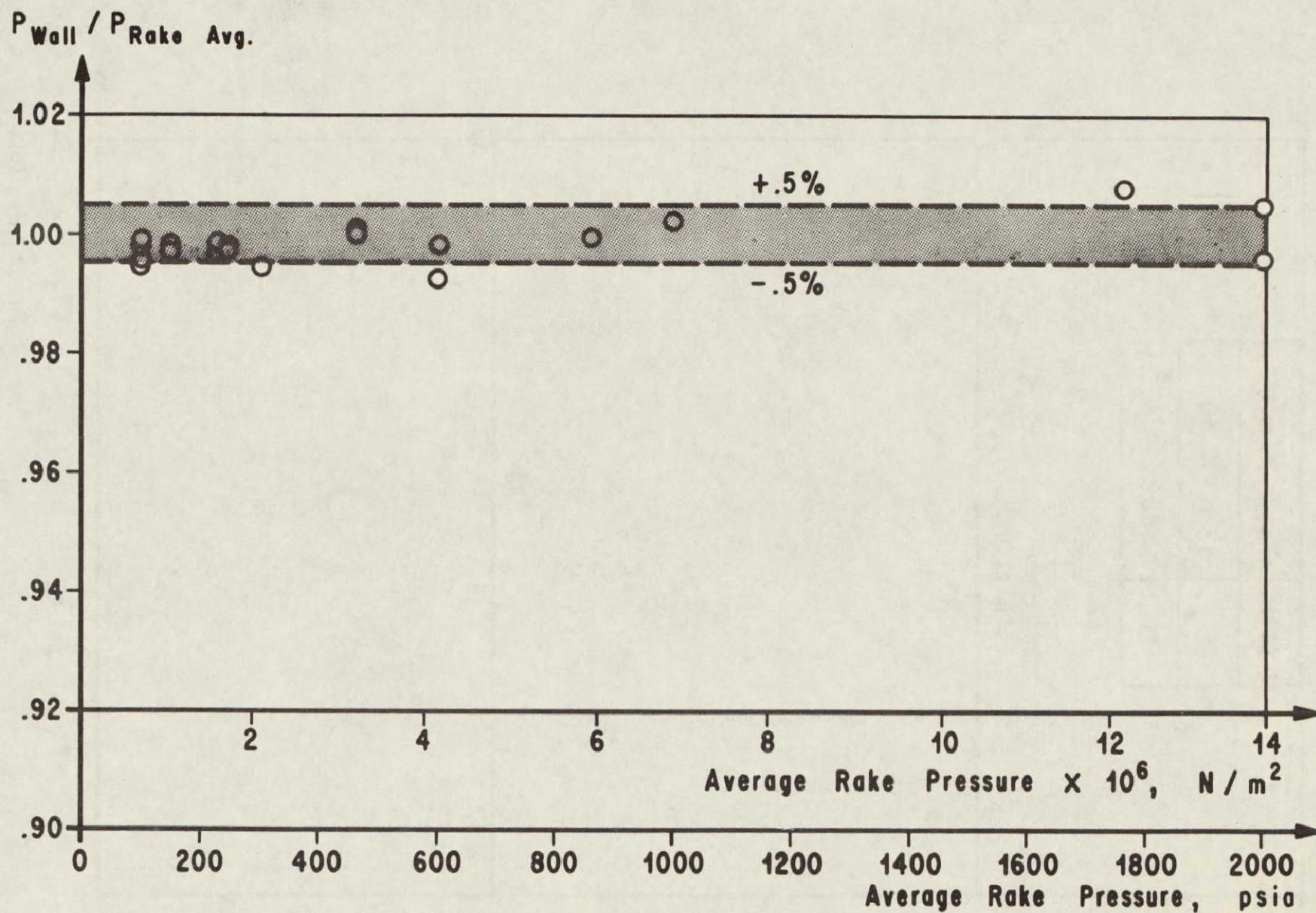


FIG. 10. RATIO OF WALL STATIC PRESSURE TO AVERAGE RAKE PRESSURE IN THE SETTLING CHAMBER

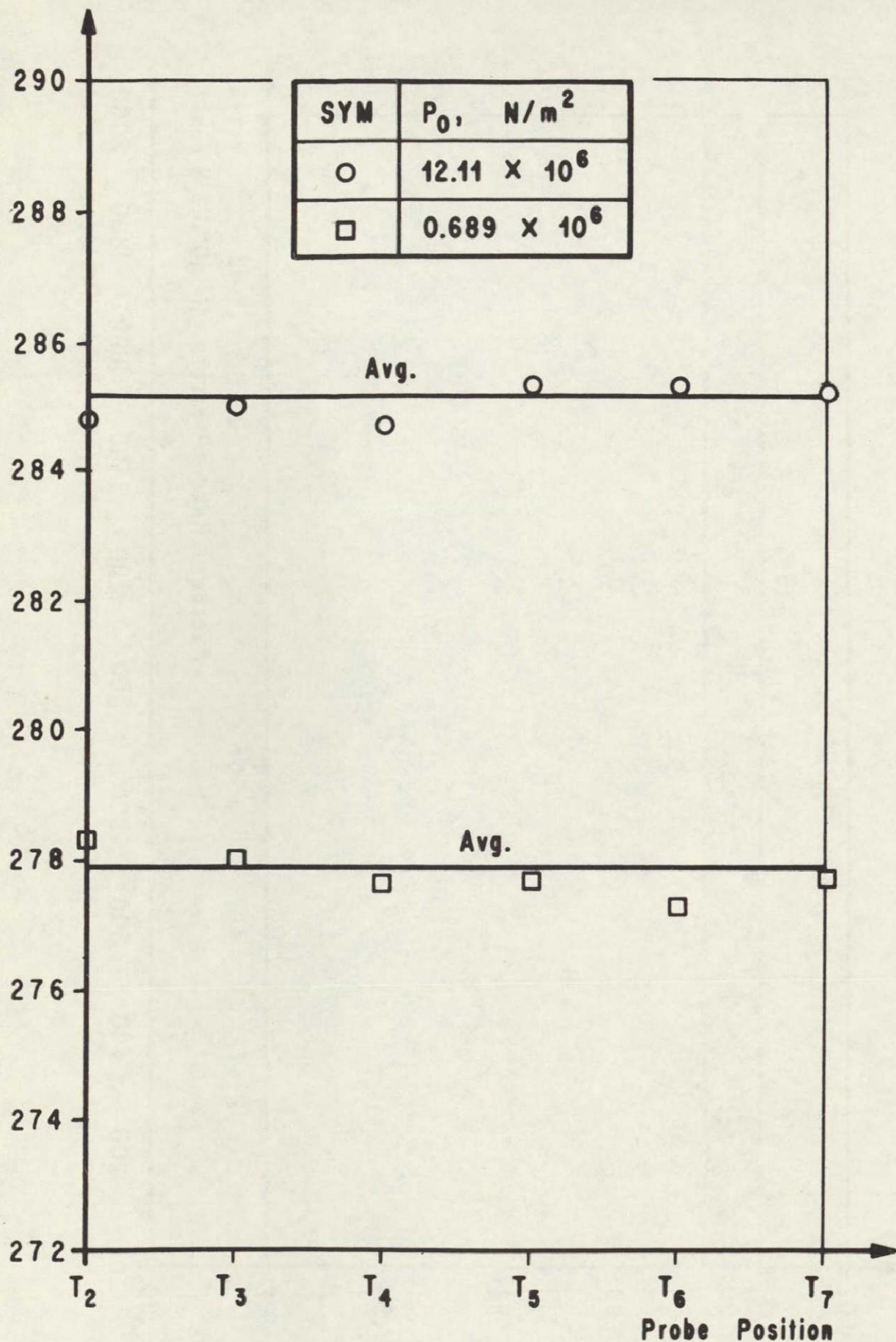
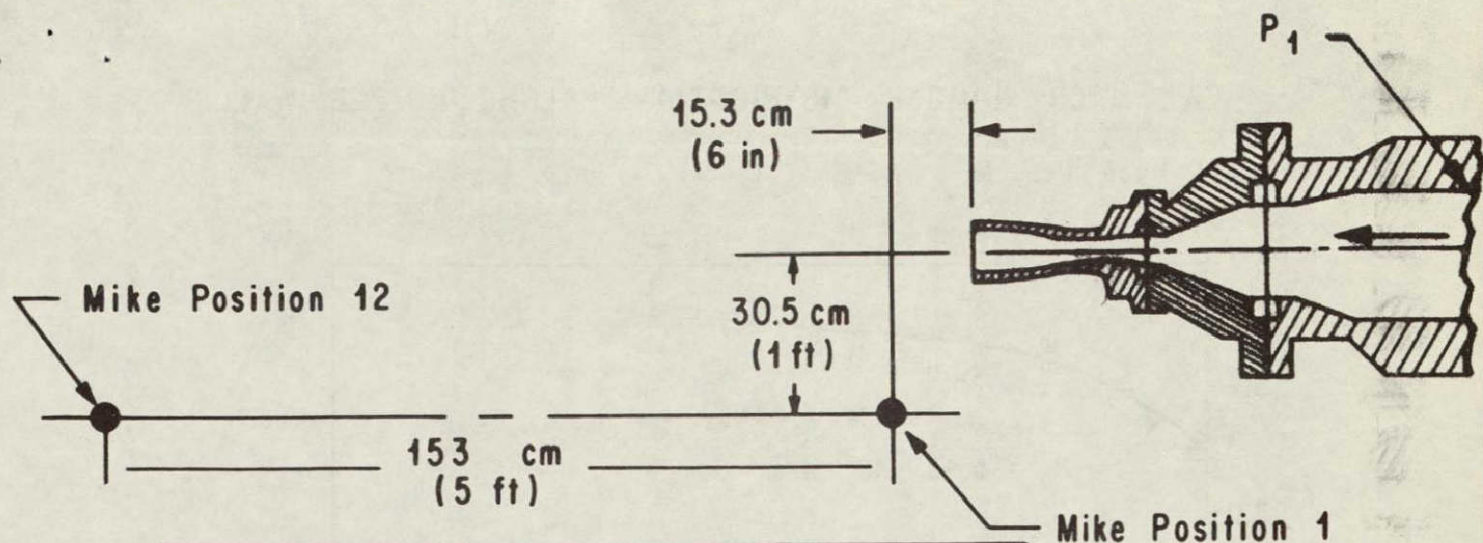


FIG. 11. STAGNATION TEMPERATURE DISTRIBUTIONS ACROSS SETTLING CHAMBER



INSTRUMENTATION
 Pressure Transducer: Kistler Model 601L
 Microphone: Bruel & Kjaer Model 4135

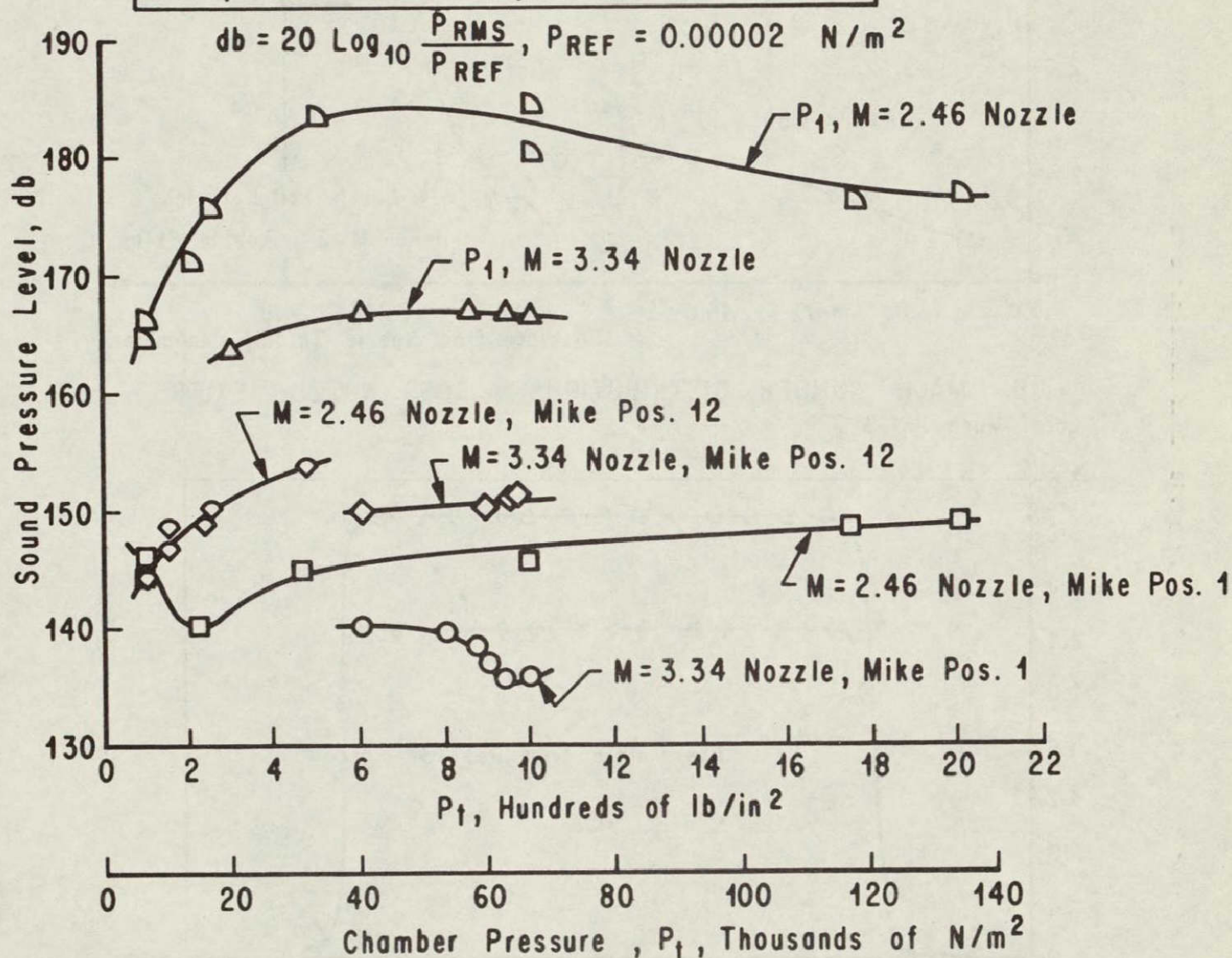
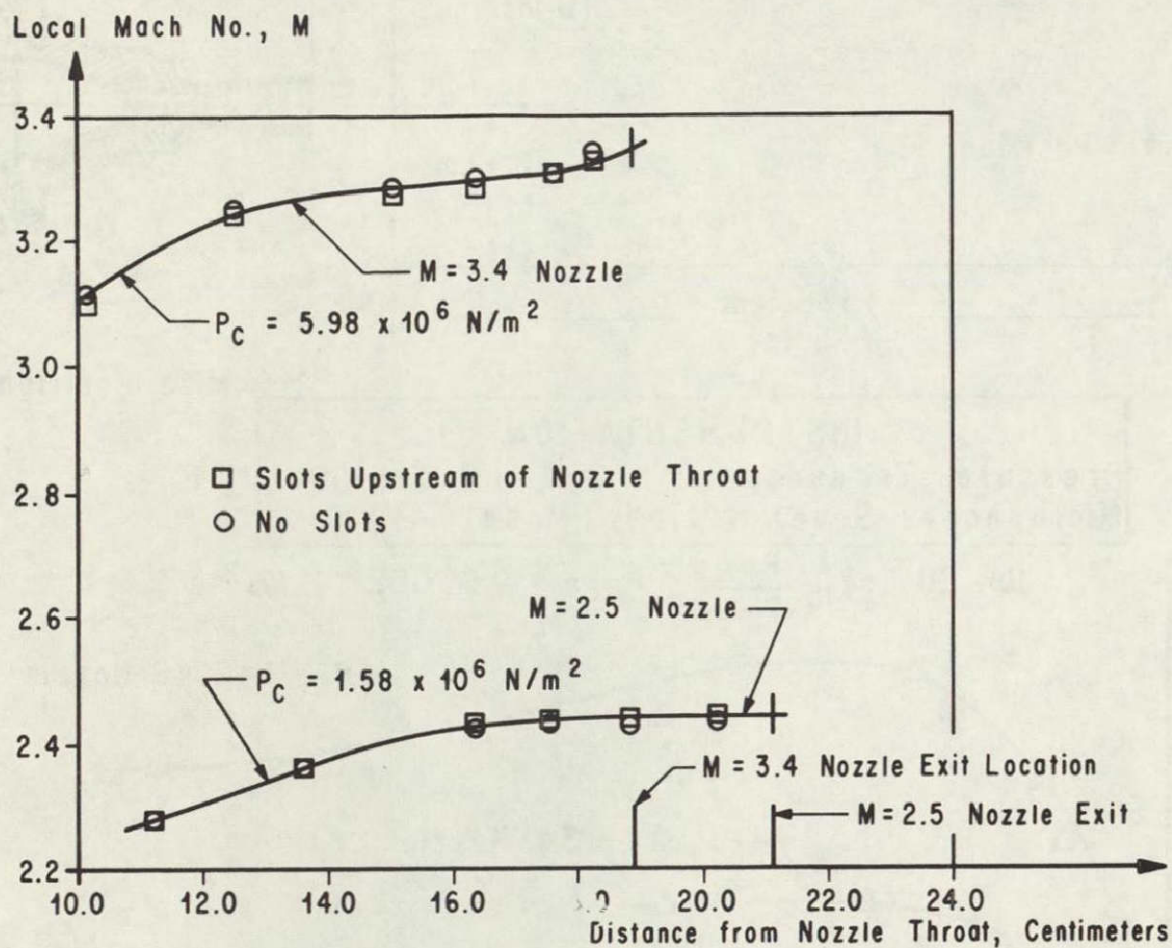
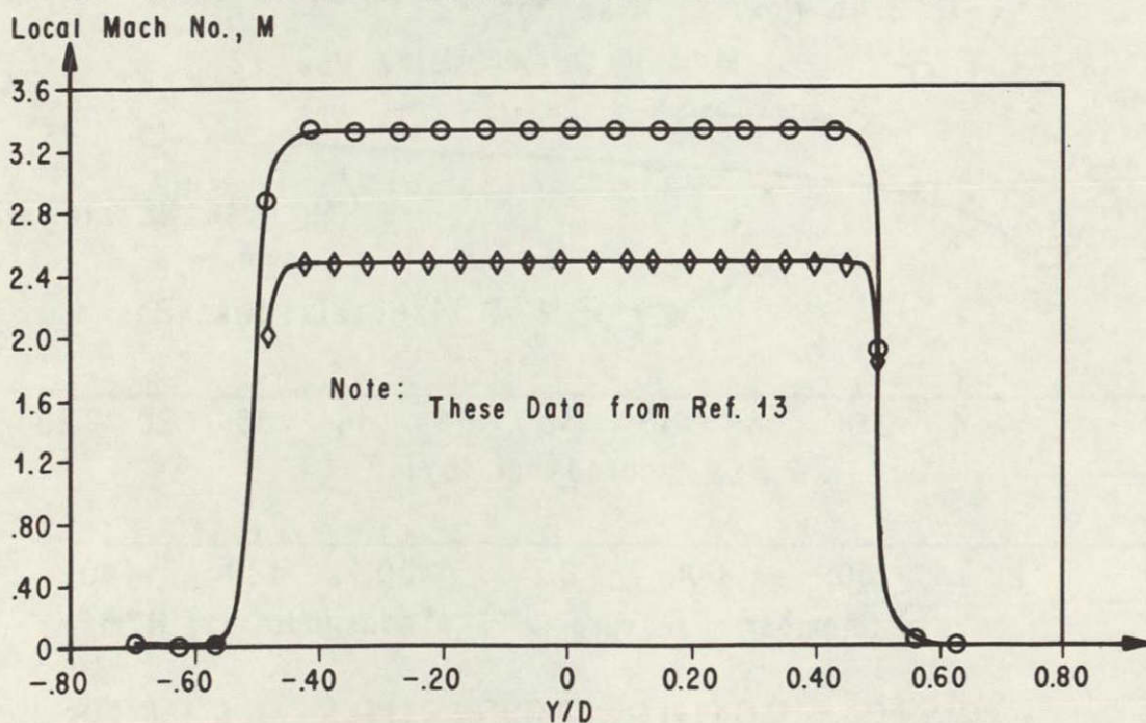


FIG. 12. SOUND PRESSURE LEVELS AT THE COLD FLOW JET FACILITY

A. MACH NUMBER DISTRIBUTIONS ALONG NOZZLE WALLS



B. MACH NUMBER DISTRIBUTIONS ACROSS NOZZLE EXITS



32 FIG. 13. MACH NO. CHARACTERISTICS OF THE NOZZLES

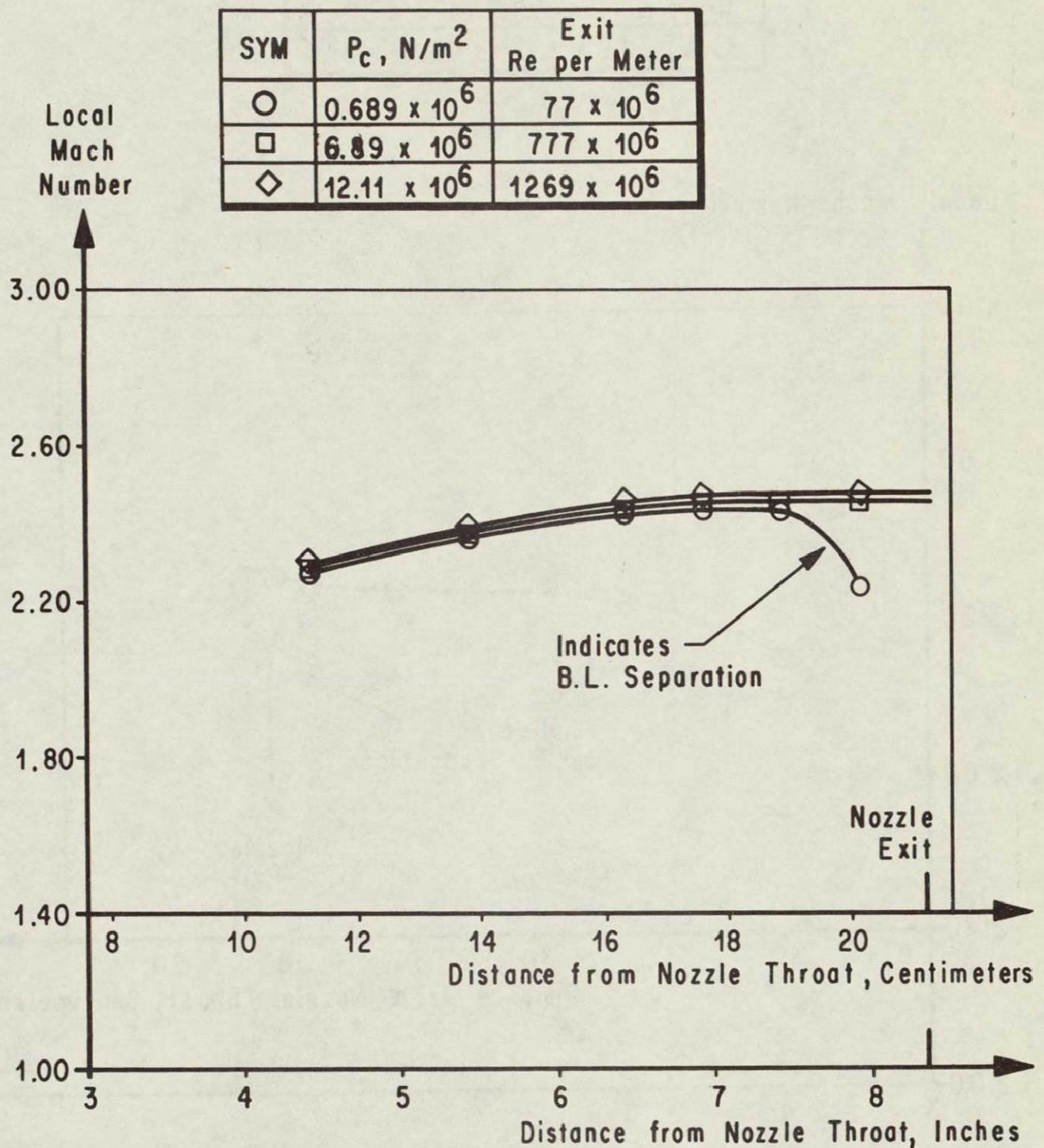


FIG. 14. EFFECT OF REYNOLDS NUMBER ON THE MACH NUMBER DISTRIBUTION IN THE NOMINAL MACH 2.46 NOZZLE

SYM	$P_c, \text{N/m}^2$	Exit Re per Meter
○	2.07×10^6	193.5×10^6
□	4.13×10^6	305×10^6
◇	5.99×10^6	430×10^6

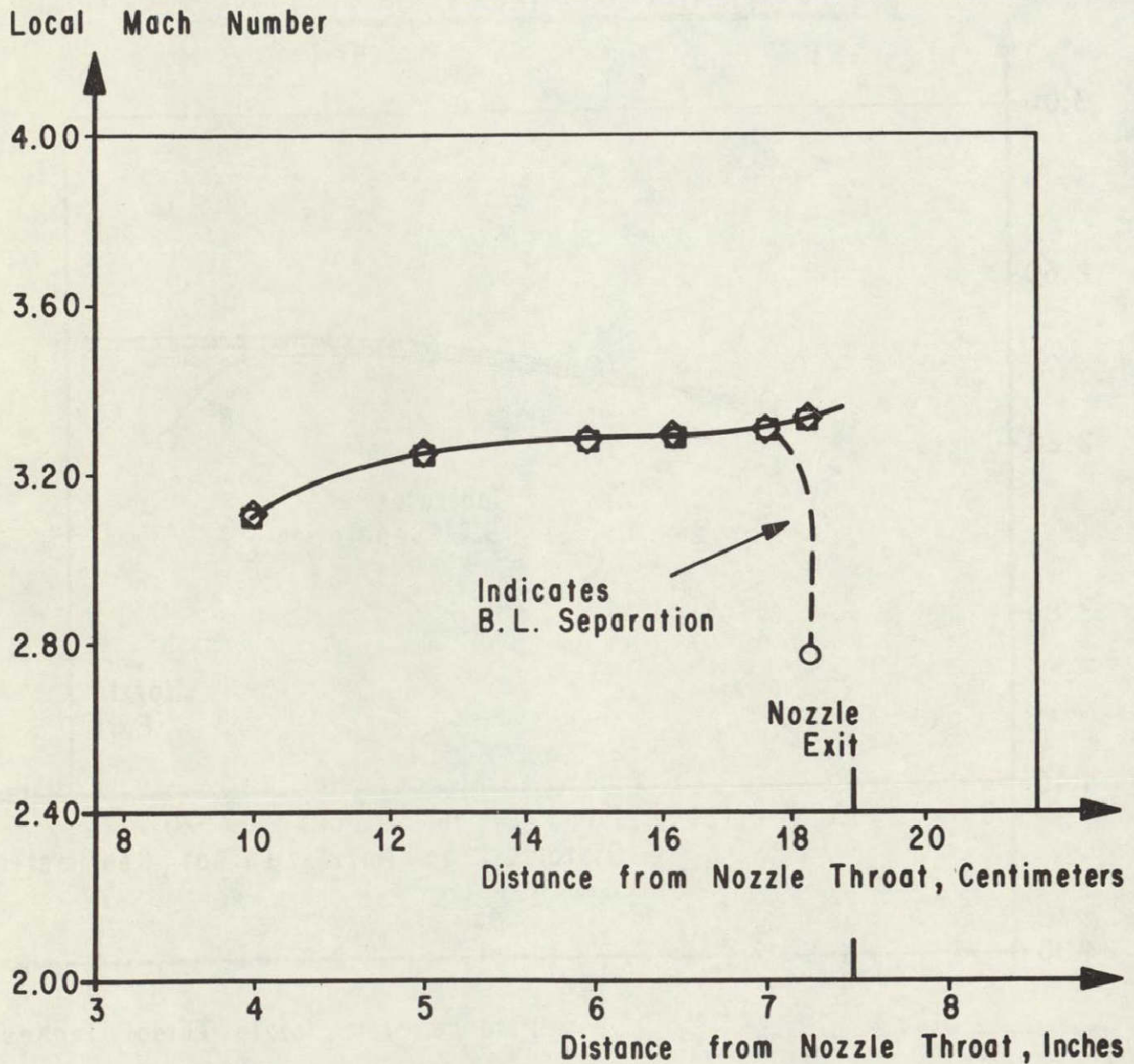


FIG. 15. EFFECT OF REYNOLDS NO. ON THE MACH NUMBER DISTRIBUTION IN THE NOMINAL MACH 3.34 NOZZLE

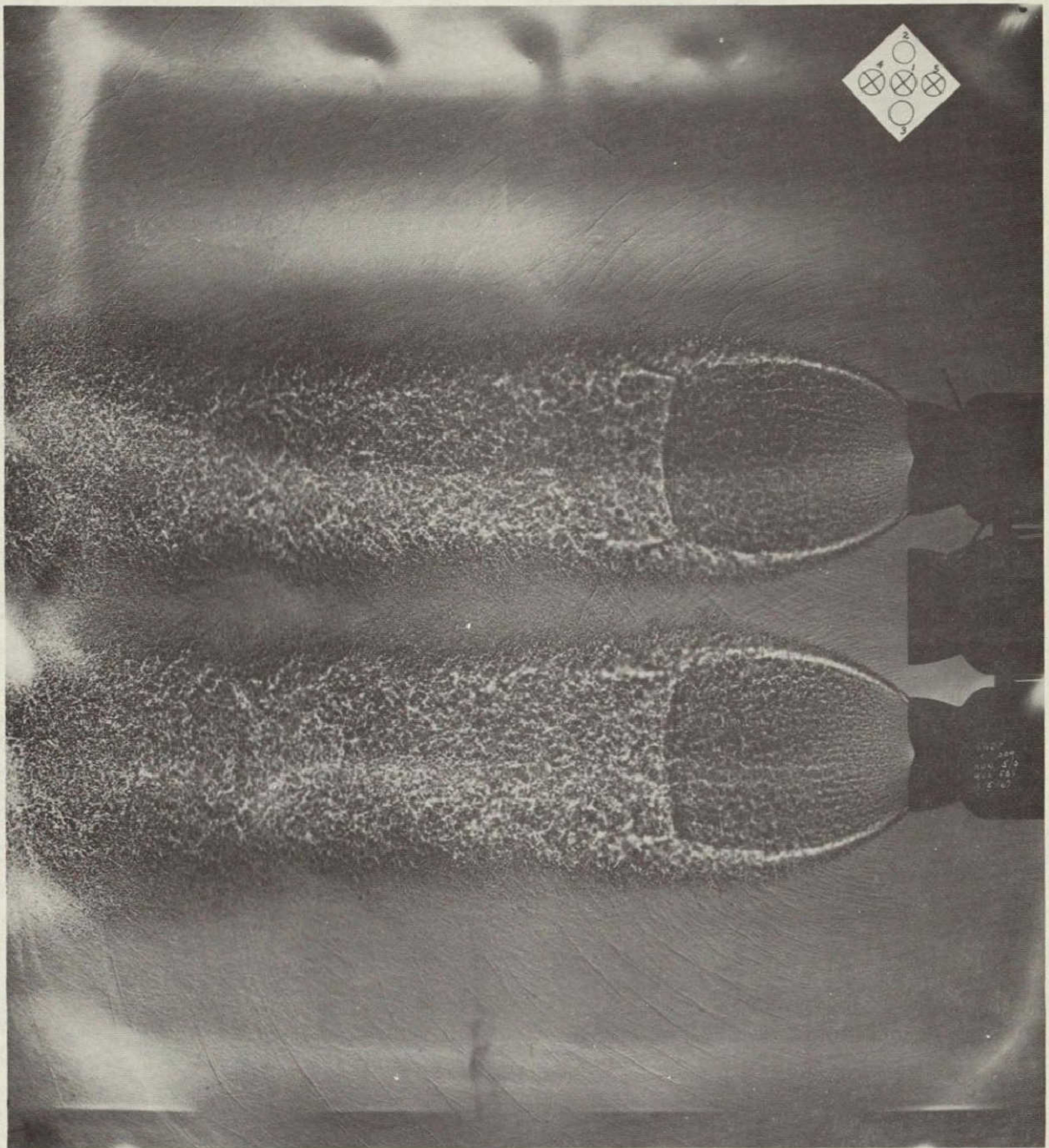


FIG. 16. SHADOWGRAPH OF CLUSTER-JET EXHAUST
 $P_0 = 6.205 \times 10^6 \text{ N/m}^2$, ENGINE 2 AND 3

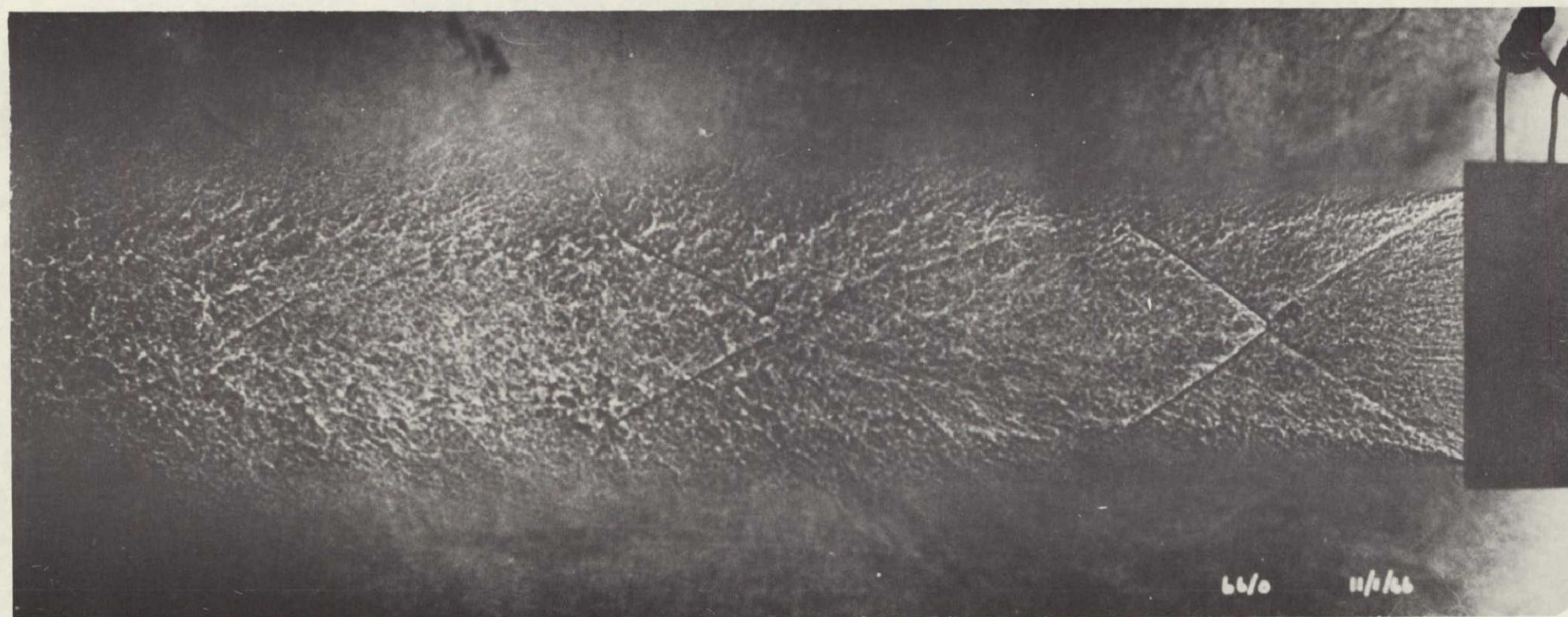


FIG. 17. SHADOWGRAPH OF JET EXHAUST
 $M = 2.5$, $P_0 = 1.03 \times 10^6 \text{ N/m}^2$ (150 psia)

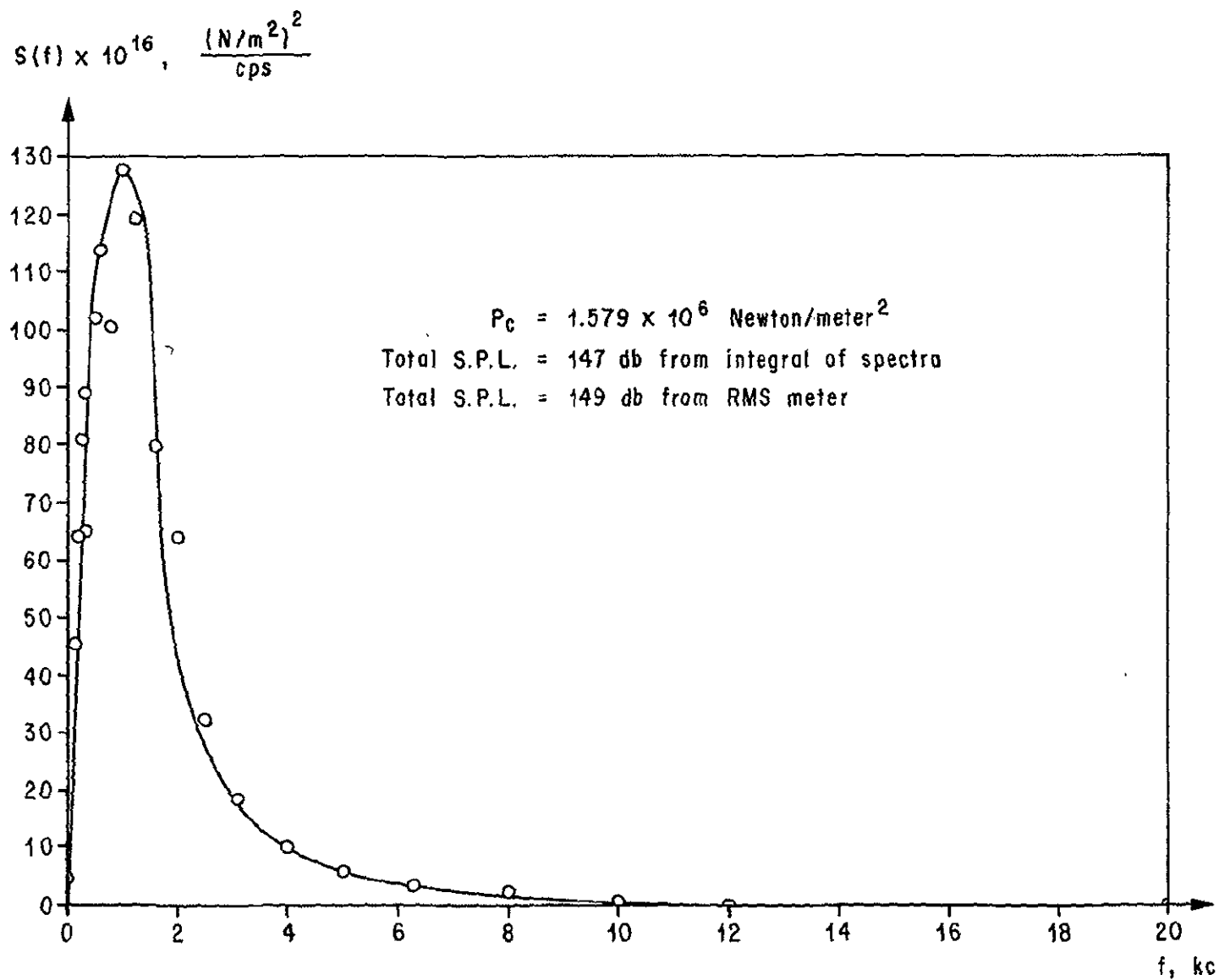


FIG. 18. POWER SPECTRUM OF JET NOISE AT MIKE LOCATION 12, M=2.46 NOZZLE

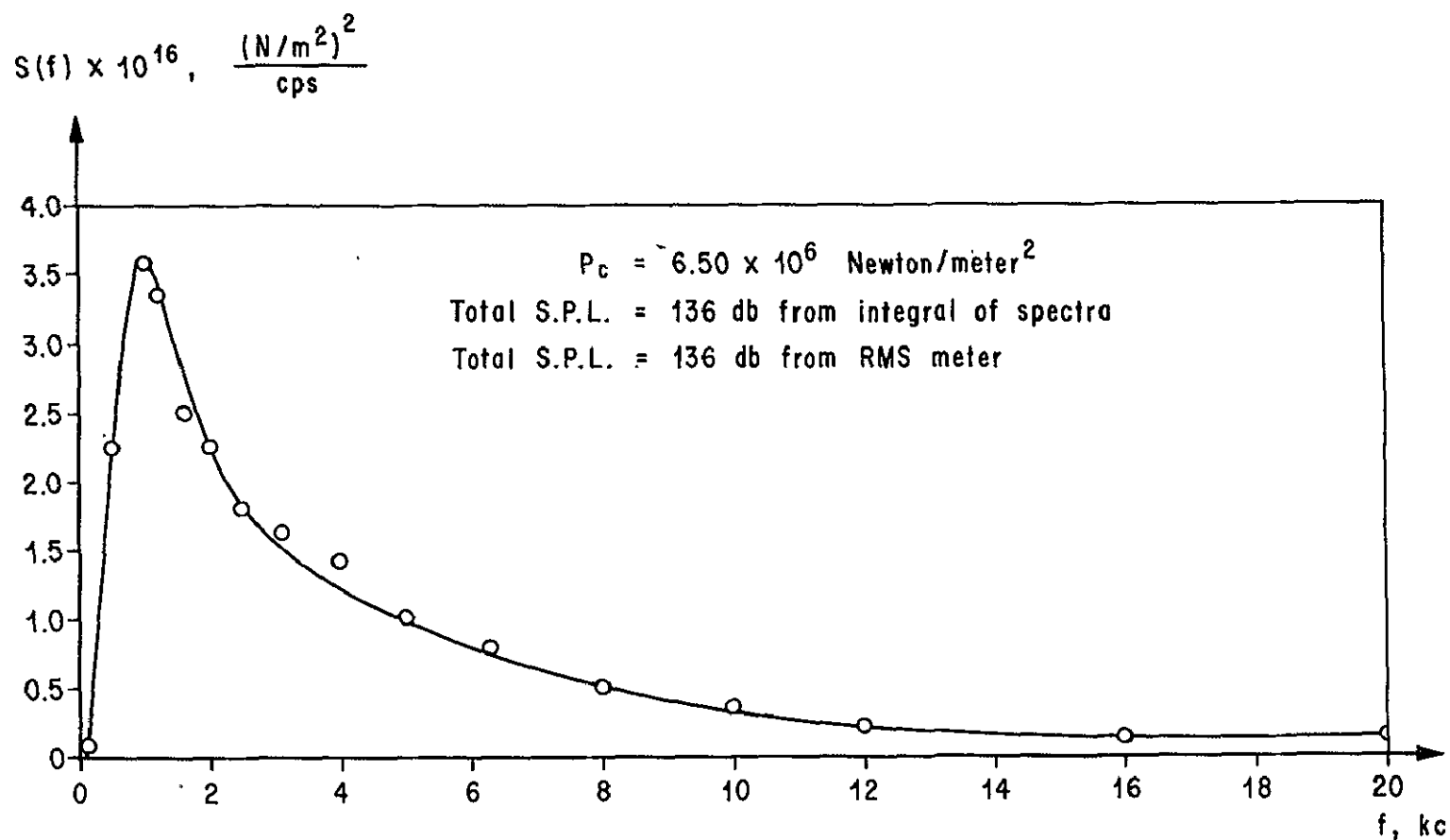


FIG. 19. POWER SPECTRUM OF JET NOISE AT MIKE LOCATION 1, $M = 3.34$ NOZZLE

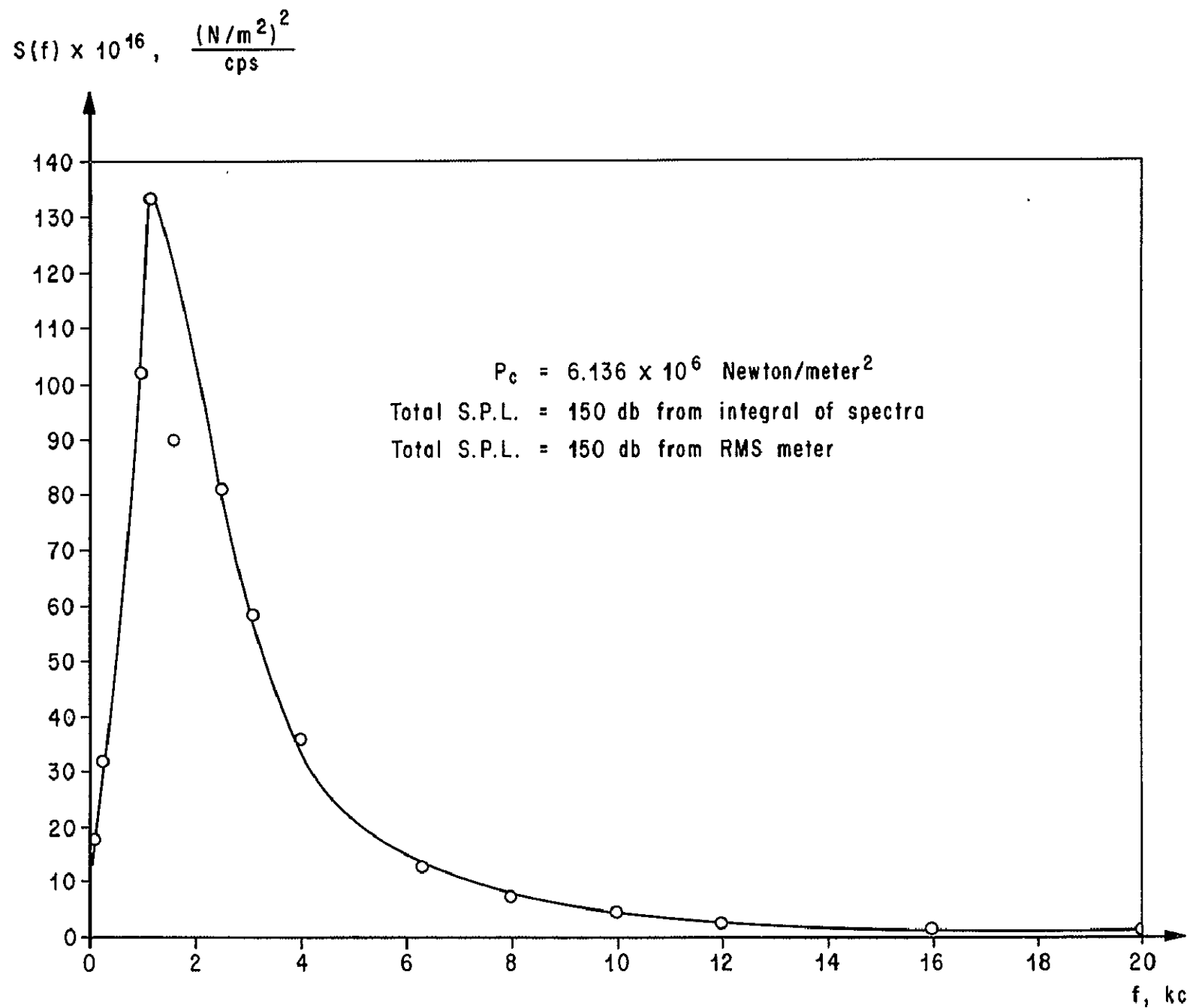


FIG. 20. POWER SPECTRUM OF JET NOISE AT MIKE LOCATION 12, $M=3.34$ NOZZLE

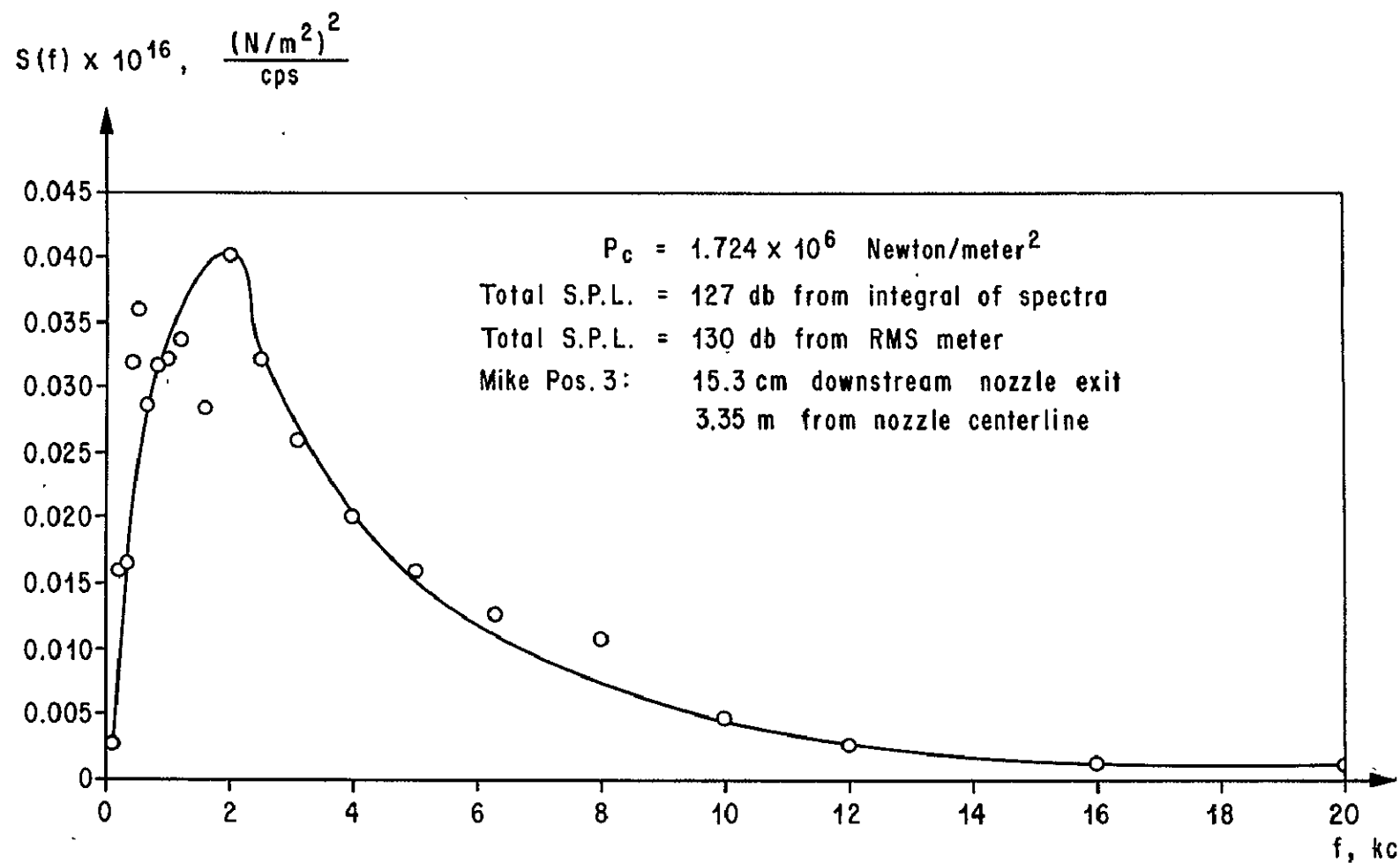


FIG. 21. POWER SPECTRUM OF JET NOISE AT MIKE LOCATION 3, $M = 2.46$ NOZZLE

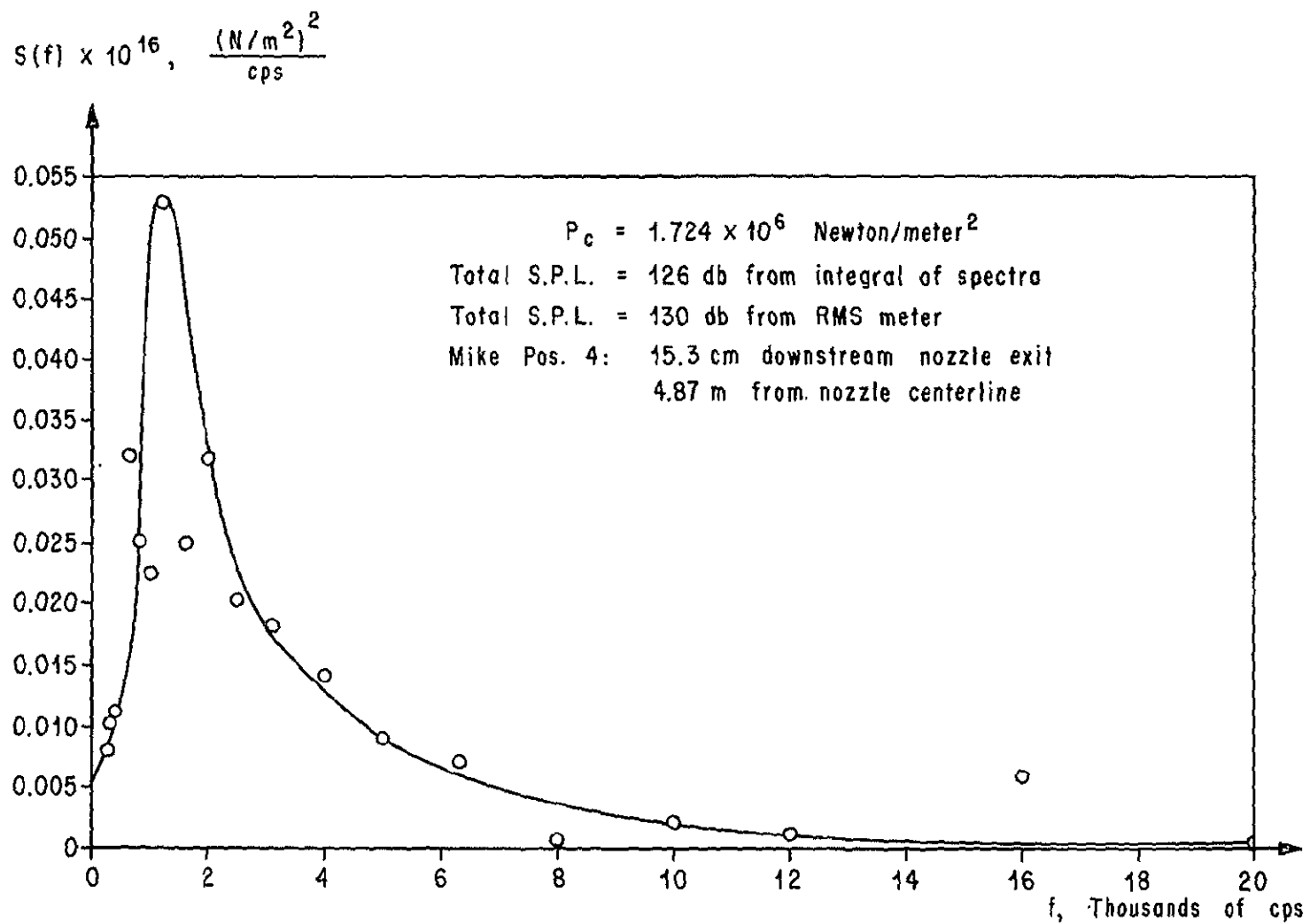


FIG. 22. POWER SPECTRUM OF JET NOISE AT MIKE LOCATION 4, M = 2.46 NOZZLE

REFERENCES

1. Johnston, K. D., "Aerodynamic Design Considerations on the Cold Flow Duct of the Thermal and Acoustic Simulation Facility," R-AERO-AM memo to Mr. Belew, Aug. 27, 1965.
2. Pankhurst, R. C. and D. W. Holder, Wind Tunnel Technique, Sir Isaac Pitman and Sons, London, 1952.
3. Batchelor, G. K., The Theory of Homogeneous Turbulence, University Press, Cambridge, 1953.
4. Batchelor, G. K. and A. A. Townsend, "Decay of Turbulence in the Final Period," Proceedings of Royal Society of Aeronautics, Vol. 194, 1948.
5. MacPhail, D. C., "Turbulence Changes in Contracting and Distorted Passages," Reports and memoranda No. 2437 (R.A.E. Report No. Aero. 1928), 1944.
6. Schubauer, G. B., W. G. Spangenberg, and P. S. Klebanoff, "Aerodynamic Characteristics of Damping Screens," NACA TN 2001, January 1950.
7. Dryden, Hugh L. and G. B. Schubauer, "The Use of Damping Screens for the Reduction of Wind-Tunnel Turbulence," Jo. of the Aeron. Sci., Vol. 14, April 1947.
8. Fisher, M. J. and K. D. Johnston, "Turbulence Measurements in Supersonic, Shock-Free Jets by the Optical Crossed-Beam Method," NASA TN (to be published).
9. Elliot, D. G., D. R. Bartz, and S. Silver, "Calculation of Turbulent Boundary Layer Growth and Heat Transfer in Axisymmetric Nozzles," JPL Report 32-387, February 1963.
10. Zinsmeyer, H. G., "Flow Analysis of Supply and Flow Regulation System on the Cold Flow Duct Assembly," Hayes Report No. 1205, Contract No. NAS8-20083, December 1965.
11. Hill, J. C., "Operators Manual on the Cold Flow Duct Assembly," Hayes Report No. 1254, Contract No. NAS8-20083, March 1966.
12. Barnett, D. O., "Spectral Characteristics of Vibration and Static Pressure Fluctuations in the Cold Flow Duct Settling Chamber of the TAJF," Northrop Report M-794-8-358, Contract NAS8-20082, June 1968.

REFERENCES (Continued)

13. Delany, B. R., and W. C. Tidmore, "Data Report of the Characteristics of a Cold Flow Free Jet Experimental Investigation," Northrop/Huntsville TR 317, April 1967.
14. Heaman, J. P., "Instrumentation for Unsteady Pressures and Accelerations Measured at the Cold Flow Jet Facility with Limited Sound Level Data," R-AERO-AE memo, November 1, 1966.

APPROVAL

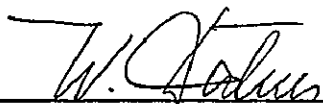
TN-AERO-69-1

AERODYNAMIC DESIGN AND CALIBRATION OF THE
MSFC THERMAL-ACOUSTIC JET FACILITY - COLD FLOW DUCT


by K. D. Johnston and W. C. Tidmore

The information in this report has been reviewed for security classification. Review of any information concerning Department of Defense or Atomic Energy Commission programs has been made by the MSFC Security Classification Officer. This report, in its entirety, has been determined to be unclassified.

This document has also been reviewed and approved for technical accuracy.



W. K. Dahm
Chief, Aerophysics Division



E. D. Geissler
Director, Aero-Astroynamics Laboratory

DISTRIBUTION

R-AERO

Dr. Geissler
Mr. Jean
Mr. Murphree
Dr. Heybey
Mr. Dahm
Mr. Holderer
Mr. Felix
Mr. Heaman
Mr. Simon (6)
Mr. Davis
Mr. Cope (6)
Mr. Neighbors
Mr. Bush
Mr. Walker
Mr. Reed
Mr. Wilhold
Mr. Howard
Mr. Walker
Mr. Schutzenhofer
Mr. Brewer
Mr. Huffaker
Mr. Linsley
Mr. Andrews
Mr. Belew
Mr. Love
Mr. Fields
Mr. Clark
Mr. Sims
Mr. Jones (6)
Mr. Ellner
Mr. Funk
Mr. Jayroe
Mr. Stephens
Mr. Huflutzel
Dr. Krause
Mr. Johnston (25)
Mr. Kadrmas
Mrs. Hightower

Northrop-Nortronics
Huntsville, Ala.
Attn: Mr. Tidmore (6)
Mr. Ryan
Mr. Barnett
Mr. Cikanek
Dr. Su
Mr. Bennett

IITRI
Chicago, Ill.
Attn: Dr. R. Damkevala (6)
Dr. R. Denmen
Dr. L. Wilson
Col. Ferrell
Dr. M. Fisher
Mr. R. Norman

MS-IP